a0005

5.06 Crustal Magnetism

M. E. Purucker, Goddard Space Flight Center/NASA, Greenbelt, MD, USA

K. A. Whaler, Grant Institute, Edinburgh, UK

Nomenclature

a	radius of Earth
$\mathbf{A}$	analytic signal
$\mathbf{B}$	magnetic induction
d	magnetic source–observation distance
$\mathbf{F}$	non-crustal magnetic field
g_n^m, h_n^m	spherical harmonic coefficients
$\mathbf{G}$	Green's function
$\mathbf{H}$	magnetic field intensity
$\mathbf{M}$	magnetization
$\mathbf{M}_i$	induced magnetization
$\mathbf{M}_r$	remanent magnetization
Ma	million years ago
P	pressure
$P_n^m(\cos\theta)$	Schmidt quasi-normalized associated Legendre functions of degree n and order m
Q	Koenigsberger ratio
s_i	structural index or attenuation rate
t	time
$\mathbf{T}$	total field
v	volume
v_f	volume fraction of magnetite
V	scalar potential
μ_0	permeability of free space
θ	colatitude
τ	temperature
ϕ	longitude
χ	magnetic susceptibility
ΔT	total field anomaly
Γ	Gram matrix

Glossary

g0005 **analytic signal** A transformation formed through the combination of the horizontal and vertical gradients of a magnetic anomaly.

g0010 **CHAMP** A low-earth orbiting satellite launched in 2001 designed to map the vector crustal magnetic field.

g0015 **crust (lithosphere)** The outer shell of the Earth formed by differentiation under the influence of temperature and gravity. The crust overlies the mantle, and the distinction can be expressed in terms of seismic velocities, rock density, rock type, mineralogy, chemical composition, or magnetic properties. The lithosphere, a rheological term, includes the crust, and the uppermost mantle.

g0020 **Curie depth** The depth at which rocks lose their permanent and induced magnetism by virtue of their elevated temperature. The Curie depth is a function of the geothermal gradient within the Earth, and the magnetic mineralogy.

g0025 **Curie temperature** The temperature at which a rock loses its permanent and induced magnetism.

g0030 **Euler deconvolution method** A technique for estimating source positions for magnetic anomalies, which relates the magnetic field to its gradient through the specification of the arrangement of the magnetic sources.

g0035 **Green's function** The relation of magnetization to magnetostatic potential.

g0040 **harmonic spline** A local basis function employed in modeling the magnetic field.

g0045 **International Geomagnetic Reference Field (IGRF)** Values for the spherical harmonic coefficients from which the magnetic field can be calculated at any point in space and time. Each IGRF consists of a set of main field and secular variation coefficients covering a 5-year interval, thereby accounting for the temporal evolution of the main field.

g0050 **Koenigsberger ratio, *Q*, or *Q*-ratio** Expresses the relation between the strength of the induced and remanent magnetizations. It is given by $|\mathbf{M}_r| \div |\mathbf{M}_i|$. Hence, *Q*'s greater than unity indicate dominance by remanent magnetization; *Q*'s less than unity indicate dominance by induced magnetization.

g0055 **induced magnetization** One of two types of magnetization, the other being remanent. Induced magnetizations are proportional in magnitude and generally parallel to the ambient field **H.**

g0060 **magnetic basement** The top of a layer of more strongly magnetized rocks, usually igneous and/or metamorphic rocks, underlying more weakly magnetized sediments.

g0065 **magnetic susceptibility** Expresses the proportionality factor relating ambient field **H** to the induced magnetization.

g0070 **magnetite** Dominant magnetic mineral, often with some Ti, in the Earth's crust.

g0075 **MAGSAT** The first satellite mission to map the Earth's vector magnetic field, including the long-wavelength crustal magnetic field.

g0080 **matched filter** Filter(s) that can then be used to decompose observed magnetic anomalies into estimates of the anomalies caused by sources at various depths. These depths are determined by a Fourier domain decomposition of the magnetic anomaly signal.

g0085 **observatory bias** The difference between the magnetic components measured at a magnetic observatory and those predicted by a geomagnetic model truncated at degree 13. This quantity is thought to reflect the higher-degree crustal magnetic field contribution, in part.

g0090 **pseudogravity transformation** Converts a magnetic anomaly into the gravity anomaly that would be caused by a density distribution exactly proportional to the magnetization distribution.

g0095 **remanent magnetization** One of two types of magnetization, the other being induced. The direction and intensity of a remanent magnetization is dependent on the origin and history of a rock.

g0100 **reduction to pole (RTP)** Transforms magnetic anomalies into the anomalies that would be caused by identical magnetic sources but with vertical magnetization and with measurement in a vertical magnetic field.

g0105 **structural index (SI)** Expresses the rate of attenuation of a magnetic anomaly. This attenuation is a function of the source geometry.

g0110 **total field anomaly** The signed scalar quantity, which is the most common measure of the Earth's crustal magnetic field.

g0115 **upward (downward) continuation** Transforms observed anomalies into the anomalies that would be observed at a higher (lower) altitude.

g0120 **Werner deconvolution** A depth to basement technique that assumes the magnetic body has a specific geometry (dike-like), and solves for the depth to the top of the body based on four or more observations of the magnetic field over the body.

s0005 # 5.06.1 Introduction

s0010 ## 5.06.1.1 Definition

p0005 Crustal magnetism is defined as magnetism originating from rocks below their Curie temperature, in the Earth's crust and uppermost mantle. The dominant magnetism is associated with igneous and metamorphic rocks, whereas sedimentary rocks generally have subordinate, but measurable magnetism. The magnetism of the ferri- and ferromagnetic materials is a function of temperature with a loss of magnetism as the materials approach their Curie temperature (typically 200–700° C). The increase of temperature with depth in the Earth means that rocks below a certain depth, termed the Curie depth, with be nonmagnetic. This depth is typically in excess of 20 km in stable continental regions.

s0015 ## 5.06.1.2 Measurement

p0010 The measurement of crustal magnetism is done utilizing total and vector field magnetometers, and associated gradiometers. The total field magnetometers exploit fundamental resonances (Primdahl[b1320], 2000) to measure the magnitude of the field, whereas the vector instruments typically utilize fluxgate magnetometers (Ripka[b1465], 2000). The magnetometers measure these fields from borehole, ground-based, marine, aerial, balloon, or satellite platforms.

5.06.1.3 Governing Equations

s0020

p0015 The magnetic induction $B^{(\eta)}(\mathbf{r}_j)$ of the η component of the magnetic field due to a magnetization distribution $\mathbf{M}$ is given by

$$B^{(\eta)}(\mathbf{r}_j) = -\hat{\mathbf{I}}_j^{(\eta)} \cdot \nabla_{\mathbf{r}_j} \int_v \left\{ \frac{\mu_0}{4\pi} \nabla_s \frac{1}{|\mathbf{r}_j - \mathbf{s}|} \right\} \cdot \mathbf{M}(\mathbf{s}) \mathrm{d}v \quad [1]$$

where $\hat{\mathbf{I}}_j^{(\eta)}$ is the unit vector in the η direction, v is the volume of the magnetized crust, and the quantity in brackets is the Green's function relating magnetization $\mathbf{M}$ to magnetostatic potential V. The subscript on the gradient (∇) operator indicates whether derivatives are with respect to observation point coordinates ($\mathbf{r}_j$) or locations within the magnetized crust ($\mathbf{s}$). The magnetization $\mathbf{M}$ is the vector sum of remanent magnetization $\mathbf{M}_\mathrm{r}$ and induced magnetization $\mathbf{M}_\mathrm{i}$.

$$\mathbf{M} = \mathbf{M}_\mathrm{i} + \mathbf{M}_\mathrm{r} \quad [2]$$

In the case of terrestrial crustal magnetic field observations, what is often measured is the total field, the magnitude of the total magnetic field without regards

to its vector direction. The total field anomaly (ΔT) is then

$$\Delta T = |\mathbf{T}| - |\mathbf{F}| \quad [3]$$

where $|\mathbf{T}|$ is the magnitude of the magnetic field, and $|\mathbf{F}|$ is the magnitude of the (largely) noncrustal field, determined from a global or regional model. If vector data are available, the total field anomaly is calculated as

$$\Delta T = \hat{\mathbf{F}} \cdot \mathbf{T} \quad [4]$$

where $\hat{\mathbf{F}}$ is the unit vector in the direction of $\mathbf{F}$. The geometry of a total field anomaly of a magnetic body dominated by induced magnetization is dependent on the geometry of the inducing field. At high latitudes an induced magnetization will give a total field anomaly high (positive) over the source, whereas at low latitudes an induced magnetization will yield a total field anomaly low (negative) over the source.

5.06.1.4 Previous Reviews

Book-length reviews include those of Langel and Hinze (1998), Blakely (1995), Lindsley (1991), Hahn and Bosum (1986), and Grant and West (1965). Shorter articles, within books or encyclopedias, have included Gubbins and Hererro-Brevera (2006), Shive *et al.* (1992), Frost (1991a, 1991b, 1991c), Reynolds *et al.* (1990c), Blakely and Connard (1989), Harrison (1987), Bosum *et al.* (1985), Haggerty (1976), and Zietz and Andreasen (1967). Reviews in journals include those of Mandea and Purucker (2005), Nabighian *et al.* (2005), Nabighian and Asten (2002), Clark (1997, 1999), Phillips *et al.* (1991), Keller (1988), Mayhew and LaBrecque (1987), Paterson and Reeves (1985), Grant (1985), Mayhew *et al.* (1985), Haggerty (1979), Hinze (1979), and Zietz and Bhattacharyya (1975). Bibliographies include Langel and Benson (1987), Hill (1986), and Reid (in preparation).

5.06.1.5 Computer Software and Online Applications

Computer software for crustal magnetic field applications includes a collection of Fortran subroutines in Appendix B of Blakely (1995) and online at http://pangea.stanford.edu/~blakely/subroutines.html.

Another software resource is the potential field software programs of the US. Geological Survey (Phillips, 1997), which can also be found online at http://pubs.usgs.gov/fs/fs-0076-95/FS076-95.html.

Matlab, C, and Fortran routines for the evaluation of spherical harmonic models are described in Olsen *et al.* (2006a) and can be found online at several sites, including http://www.dnsc.dk/Oested/Field_models, and from the National Geophysical Data Center at http://www.ngdc.noaa.gov/seg/geomag/models.shtml. Programs for high-degree spherical harmonic analysis (SHA) and synthesis (Adam and Swarztrauber, 1997) are associated with Spherepack, available at http://www.cisl.ucar.edu/css/software/spherepack. Occasionally, the journal *Computers and Geosciences* includes articles of relevance. The 'Numerical Recipes' C and Fortran books (Press *et al.*, 1992, 1996, 1997) are another resource for inverse codes, sparse matrix theory, wavelets, interpolation, and Fourier and spectral applications. The publicly available generic mapping package (GMT) is useful for both producing maps, and for analysis of potential field data. It is documented in Wessel and Smith (1998) and available online from http://gmt.soest.hawaii.edu. Commonly used commercial codes include Geosoft, Matlab, and IDL.

Online applications include those for the evaluation of the International Geomagnetic Reference Field (Maus and Macmillan, 2005), available from the NGDC website at the address above. Along these same lines, there is also available an application for the evaluation of the CM4 Comprehensive Model (Sabaka *et al.*, 2004) at http://planetary.mag.net. Finally, the Atlas of Structural Geophysics (Jessel, 2002) can be found online at http://www.mssu.edu/seg-vm/exhibits/structuralatlas.

5.06.1.6 Structure of the Remainder of the Chapter

The remainder of this chapter begins with a summary of the salient points of magnetic petrology. We then outline the utility of crustal magnetism through a series of case studies, and discuss compilations to produce models at continental or larger scale. This is followed by details of the processing, transformation, and modeling methods that are applied to crustal magnetic data to facilitate interpretation. The issue of the separation of the various contributions to the measured magnetic field is then addressed, and we conclude with one of the key outstanding questions, identifying the induced and remanent components of magnetization.

5.06.2 Magnetic Petrology

An understanding of the processes that create, alter, and destroy magnetic minerals in rocks is the province of magnetic petrology (Lindsley, 1991; Clark, 1997). This field integrates rock magnetism (*see* 00093) and petrology to address questions such as the effects of metamorphism, hydrothermal alteration, rock composition, and redox state on magnetic properties. Magnetic minerals of major importance to an understanding of crustal magnetism are the Fe–Ti spinel group (magnetite and titanomagnetite), the rhombohedral titanohematites, and monoclinic pyrrhotite. These minerals can possess remanent (permanent) or induced (in response to an inducing field) magnetizations. Induced magnetization is, to first order, proportional to, and parallel to the direction of, the inducing field. The proportionality constant χ is called the magnetic susceptibility, and the governing relationship is of the form $|\mathbf{M}| = \chi|\mathbf{H}|$. Magnetic susceptibility in many rocks in strongly controlled by their magnetite content and the empirically determined relationship (Shive *et al.*, 1992) is

$$\chi \approx 0.2 \times 4\pi v_f \quad [5]$$

where χ is the susceptibility and v_f is the volume fraction of magnetite. Many authors use k for susceptibility.

Magnetic remanence, on the other hand, while also correlated with titanomagnetite content, is strongly dependent on the grain size, shape, and microstructure of the magnetic minerals. The Koenigsberger ratio (Q) measures the relative strengths of the induced and remanent magnetizations. It is given by $|\mathbf{M}_r|/|\mathbf{M}_i|$. Hence, Q's greater than unity indicate dominance by remanent magnetization; Q-values of less than unity indicate dominance by induced magnetization. Representative tables and values of susceptibility and Q can be found in Clark (1997).

The magnetic properties of igneous and metamorphic rocks are a reflection of the partitioning of iron between oxide and silicate phases, and do not correspond to standard petrologic classifications. This partitioning occurs in the near-surface realm (Clark, 1997) and probably also within the deep lithosphere (cf. Wasilewski and Mayhew, 1992). Standard sedimentary rock classifications, on the other hand, do show a correspondence with magnetic properties. Fe-rich chemical sediments (e.g., banded iron formations) and immature clastic sediments with abundant magnetite are two strongly magnetic sedimentary rock types, for example. Iron sulfide minerals, possibly associated with hydrocarbon migration or abiologic processes, may also produce subtle magnetic anomalies over sedimentary basins (Reynolds *et al.*, 1991, 1994), but the active processes are still controversial and an active area of research (Stone *et al.*, 2004).

Igneous and metamorphic rock types (e.g., granodiorite, rhyolite, and gabbro) often exhibit bimodal susceptibility distributions, a reflection of ferromagnetic and paramagnetic populations (cf. Figure 7 in Clark, 1999). This was first recognized as a consequence of the very large petrophysical sampling program conducted on the Fennoscandian shield (cf. Korhonen, 1993). Iron in the paramagnetic population is incorporated into silicate phases, whereas iron in the ferromagnetic population is typically in magnetite.

The magnetic petrology of granitic rocks provides an example of this bimodal distribution, with the relatively oxidized, magnetite-rich, I-type granitoids contrasting with the relatively reduced, ilmenite-rich, S-type granitoids (Clark, 1999). These granitoid types can often be distinguished by the presence of common minor minerals. Hornblende–biotite granodiorites are usually ferromagnetic, whereas muscovite–biotite granodiorites are not (Clark, 1997). Economic mineralization (Cu, Au, Mo, Sn) also shows patterns (Ishihara, 1981) that are controlled in part by this classification.

Although the rule of thumb that basic rocks are more magnetic than silicic rocks is often violated, rocks from within a single igneous province are more likely to show this tendency than are larger population samples. Hence, interpretation of magnetic surveys should include investigation of the magnetic properties of representative rock samples when possible. Within-province generalizations also find that basalts have slightly higher susceptibilities than related andesites, but phonolites are weakly magnetic. Rhyolites also exhibit a bimodal susceptibility distribution. Rhyolites which are under- or oversaturated with respect to alumina, or which contain iron-rich olivine, are likely to be weakly magnetic (Clark, 1999).

Rapidly chilled basaltic rocks are characterized by high Q-values, and the Q-ratio is strongly correlated to the distance from the chilled margin. As long as the primary remanent magnetization has not been chemically or thermally modified, even relatively thick sills and dikes have high Q-values.

p0075 Hydrothermal alteration generally destroys magnetite, and replaces it with paramagnetic phases like zeolites, clays, or more weakly magnetic minerals like titanohematite (b0320 Criss and Champion, 1984). One major exception to this generalization is that serpentinization of olivine-rich ultramafic rocks produces abundant magnetite with low Q-values (b1390 Saad, 1969). Other notable exceptions include potassic alteration associated with magnetic felsic-intermediate intrusives (b1540 Sexton *et al.*, 1995) and potassic and sodic alteration in deeper levels of iron-oxide copper–gold systems (b0645 Hitzman *et al.*, 1992). Production of hydrothermal magnetite is enhanced in mafic protoliths.

p0080 Metamorphism can produce marked changes in magnetic properties, and these changes are dependent on the composition of the protolith, and the pressure (P), temperature (τ), and time (t) path of the metamorphism. For mafic igneous protoliths undergoing regional metamorphism, primary magnetite remains unchanged during zeolite to prehnite–pumpellyite grade metamorphism in the absence of hydrothermal fluids. Subsequent metamorphism to greenschist grade converts the magnetite to chlorite, epidote, and hematite. In turn, these minerals give way to biotite and amphibole in the amphibolite facies of regional metamorphism. Magnetite is again created during granulite-grade metamorphism. At the highest metamorphic grade (eclogite), the iron returns to silicates such as clinopyroxene and garnet. For sedimentary protoliths, the redox conditions prevailing during sedimentation and diagenesis, and the iron content of the protolith, constrain the mineral assemblage produced during metamorphism.

p0085 The magnetic state of the lower crust remains poorly known. Although P and τ can be predicted, the protolith's history and current compositions are the subject of speculation. Because of the lower crust's elevated temperature, induced and viscous remanent magnetizations are expected to be strong (b1555 Shive *et al.*, 1992). Inferences from deep drilling and seismic constraints suggest a generally mafic composition. A host of mineralogic and magnetic changes may occur, with maximum magnetizations in the granulite facies zone. Stable large remanence in ilmenite–hematite intergrowths (b0995 McEnroe *et al.*, 2001; b0990 b1000 McEnroe, 2001; McEnroe and Brown, 2000) within granulite-facies rocks provides another mechanism for producing magnetic rocks within the lower crust.

p0090 Two mechanisms have been suggested for large-scale magnetizations within the mantle. The conversion of metabasalt to eclogite within subducting oceanic crust releases large amounts of water into the surrounding upper-mantle peridotite, and may produce serpentinite (b0670 Hyndman and Peacock, 2003). As long as the mantle wedge in the subduction zone is cooler than the Curie temperature, it is possible that a significant magnetization may form. b0140 Blakely *et al.* (2005) have explained the long-wavelength aeromagnetic and gravity fields above the Cascadia forearc as an example of this process, using matched filters (Section 5.06.5.5.2.2) to establish the depth of the source, and a pseudogravity transform (Section 5.06.5.4.3) to center the magnetic fields over their source. Satellite magnetic anomalies over subduction zones are also common (cf. b0255 Clark *et al.*, 1985; b1715 Vasicek *et al.*, 1988, b1330 Purucker and Ishihara, 2005; b0930 Maus *et al.*, 2006), and may have a similar explanation. A second mechanism for magnetizations in the mantle invokes the presence of metallic alloys, which have been detected in xenoliths originating from the upper mantle (b1685 Toft and Haggerty, 1988). Significant amounts of metal alloys in the upper mantle could impart magnetic behaviors to depths of almost 100 km. But questions remain about how representative of the upper mantle these metal alloys are (b0415 Frost and Shive, 1989; b1690 Toft and Haggerty, 1989).

p0095 While magnetic petrologic approaches have provided significant insights into the interpretation of crustal magnetism, there still remains the problem of extrapolating from field observations at micron- to hand-sample scale to scales appropriate for aeromagnetic or satellite observation. For example, even within the ferromagnetic population, the distribution of magnetization or susceptibility is usually log normal, and exhibits high variability. b1170 Parker (1991) has developed an inverse approach, which incorporates this variability into the creation and testing of a magnetization model. Some of this high variability can also be ascribed to surface processes, such as lightning (b1725 Verrier and Rochette, 2002) and weathering, which may not be observable from non-ground-based platforms.

5.06.3 Continental and Oceanic Magnetic Anomalies

s0045

p0100 Because magnetic oxide or sulfide-bearing phases are commonly associated with other economic mineral phases, magnetic measurements play a significant role in mineral exploration. Mapping of the crustal magnetic field is a geologic and exploration tool in the terrestrial environment, and provides a third

dimension to surface observations of composition and structure. The magnetic method also contributes to plate tectonic theory, oil and gas exploration, structural geology, and geologic mapping. The generation of new seafloor at the ridge crest was established via the magnetic method. The symmetry of the magnetic patterns (Vine and Matthews, 1963) about the ridge crest is often cited as the breakthrough which led to the widespread acceptance of plate tectonics. The magnetic time scale (Heirtzler *et al.*, 1968), suitably calibrated with numerical ages, serves many purposes in the Earth sciences. In particular, readers are referred to 00091 for further details of crustal magnetism within the oceanic realm. Inferences from crustal magnetic fields, interpreted in conjunction with other geological and geophysical information, can locate kimberlite pipes, impact structures, plutons, ophiolites, and other geologic entities which have a magnetic contrast with their surroundings. This permits extrapolation from, or interpolation between, outcrops, drill holes, or regions of localized geophysical measurements into areas where surficial materials may obscure the feature. Magnetic studies can locate faults, folds, and unconformities, and describe their geometrical properties. Magnetic measurements provide constraints on the amount of sediment in a depositional basin by characterizing its depth and dimensions. Magnetic measurements can be used to infer heat flux, and the depth to the bottom of the magnetic crust, because magnetic properties are temperature dependent. Finally, crustal magnetic fields can help delineate suture zones or terrane boundaries, and unravel the history of volcanic terranes.

p0105 In the sections that follow, we use a case study approach to illustrate the utility of the magnetic method. We begin with the Chicxulub impact structure, showing how it was first recognized using a combination of aeromagnetic and gravity data, and how these data sets have been used to produce three-dimensional (3-D) models of the structure. We proceed then to review geodynamical interpretations of aeromagnetic data that have been derived from dike swarms, and some of the caveats that must be considered. We then discuss structural and tectonic interpretations of aeromagnetic maps over forearc basins with Cenozoic to Recent faulting, and their role in assessing earthquake risk. We next illustrate how magnetics has been used to infer heat flux under the Antarctic ice cap, and how this may have applications in modeling ice flow, and in identifying undiscovered volcanic regions under the ice. In the exploration arena, we summarize the role of aero- and ground magnetic surveys in identifying diamond-bearing kimberlites from northern Canada. Finally, we review the structural inferences drawn from magnetic and gravity surveys over the West Siberian Basin, and their relation to the world's largest gas field, the Urengoy. A case study approach such as this might also have included a demonstration of the utility of magnetics in determining the depth to basement in sedimentary basins, and its relevance in petroleum exploration. The proprietary nature of this kind of work means that while there are no shortage of articles discussing depth to basement techniques (e.g., Peters, 1949; Li, 2003; Thompson, 1982; Thurston *et al.*, 2002; Thurston and Smith, 1997; Hsu *et al.*, 1998; Ku and Sharp, 1983; Mushayandebvu *et al.*, 2001; 2004; Naudy 1971; Salem and Ravat, 2003; Silva *et al.*, 2001, 2003; Nabighian *et al.*, 2005), there is only a single volume (Gibson and Millegan, 1998) which focuses on the role of magnetics in an integrated hydrocarbon exploration program. AU8

5.06.3.1 Chicxulub s0050

p0110 Located below, and straddling the coastline of the northwest Yucatan, Mexico, the Chicxulub impact structure (**Figure 1**) is the world's most widely known impact, and produced major biologic and environmental changes at the end of the Cretaceous Period 65 Ma. The enhanced porosity associated with the collapse of nearby structures (Grieve and Therriault, 2000) from Chicxulub's associated seismic events has been linked to the development of large hydrocarbon deposits in the Campeche Bank region immediately to the NW. The impact site is now covered by up to 1 km of carbonate rock. First recognized by its circular and coincident magnetic (**Figure 1**) and gravity signatures in the aftermath of a 1978 survey (Penfield and Camargo, 1981), the impact was subsequently tied to other diagnostic signatures such as an iridium anomaly and shocked quartz grains by direct drilling into the structure, and dating of the crystallization age of the melt rocks (Hildebrand *et al.*, 1991; Sharpton *et al.*, 1992).

p0115 The magnetic signature consists of three concentric zones (Pilkington and Hildebrand, 2000) with radii of 20, 45, and 80 km. The impact occurred in a carbonate sequence several kilometers thick characterized by much longer (hundreds of kilometers) and weaker amplitude magnetic anomalies. The innermost zone is characterized by a single, high-amplitude anomaly

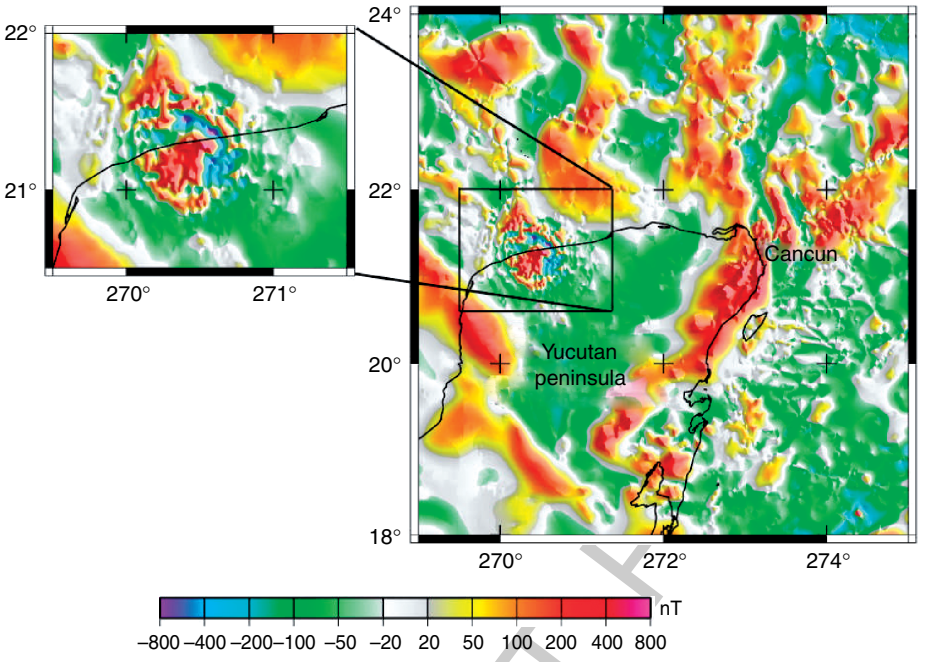

f0005 **Figure 1** Total field anomaly (ΔT) over Chicxulub impact structure (Pilkington and Hildebrand, 2000), shown in an expanded view in the inset. Coastline is shown as a solid line. Data interpolated to a 1-km grid from digital data grids of the magnetic anomaly map of North America (Bankey *et al.*, 2002). Artificial illumination from the NNE and ESE. Mercator projection.

indicative of a single source. The middle zone consists of numerous, intermediate-amplitude dipolar anomalies. The outermost zone consists of short-wavelength, low-amplitude anomalies. The outermost zone is better defined by its gravity signature, and associated cenotes (freshwater caves), than by its magnetic signature. In their recent interpretation of the aeromagnetic survey data, Pilkington and Hildebrand (2000) perform 3-D modeling of the crater structure by inversion using a two-layer model. The layers, at depths corresponding to the melt sheet and the basement surface, are inverted individually subsequent to separation via a wavelength filter (see Section 5.06.5.5.2.2 for the related concept of matched filter). The inner magnetized zones within the melt sheet are interpreted to result from hydrothermal activity at the edge of the central uplift and the collapsed disruption cavity. Although some lines of evidence (Snyder *et al.*, 1999) suggest that Chicxulub may be a multi-ring impact structure, the magnetic data as currently modeled resolve only a single ring with a central peak. Although the magnetic signature of Chicxulub is distinctive, a variety of magnetic signatures are encountered in other terrestrial impact structures (Pilkington and Grieve, 1992; Grieve and Therriault, 2000; Shah *et al.*, 2005; Goussev *et al.*, 2003), dependent on the target rocks, impact magnetizations, and subsequent evolution of these metastable assemblages. A magnetic low is frequently encountered, due to a reduction in magnetic susceptibility. Large structures such as Chicxulub tend to exhibit a central high-amplitude anomaly. Imaging techniques that emphasize the edges of magnetic bodies via derivatives, or via artificial illumination in one or more directions (Wessel and Smith, 1998) are commonly employed adjuncts to magnetic-survey interpretation of impacts. Specific extensions to impact, and other circular features (e.g., kimberlite pipes) within magnetic data, are circular sunshading as described by Cooper (2003) and Cooper and Cowan (2003), and fractional derivatives (Cowan and Cooper, 2005) for better matching to the available data.

5.06.3.2 Dike Swarms

s0055

The Earth hosts hundreds of radiating, arcuate or linear mafic dike swarms (Emst *et al.*, 1996) whose mapping has contributed to improved geodynamic models of the Earth. In southern Africa alone, one digital database (Mubu, 1995) has enumerated 14 000 dikes, mapped in large part because of their magnetic expression. While some of these dikes are exposed,

p0120

most are not, and hence the magnetic method has played a crucial role in their understanding. These magnetically defined dike swarms have been used in global plate reconstructions, and locally to understand the kinematics of rifting. In addition, dikes define fractures and shear zones (**Figure 2**), along which economic mineralization is often found.

p0125 Mafic dikes provide evidence for magmatic activity, large igneous provinces, and mantle plumes (Ernst and Buchan, 2001), and are especially useful in older rocks where erosion has removed much of the other evidence for igneous activity. In these older rocks it is frequently only the dikes, representing the igneous plumbing system, that survive. Although dikes are often interpreted as paleo-stress markers, they can also reflect the pre-existing structure of the lithosphere. The Jurassic dikes of southern Africa (Reeves, 2000; Chavez Gomez, 2001; Marsh, 2005), one of the manifestations of the Karoo large igneous province, have been used to enumerate plate motion associated with the breakup of Gondwana. For example, Ernst and Buchan (1997) make the case that the convergence point of these Jurassic dikes defines the location of a paleoplume. The dikes here consist of four distinct swarms: the Okavango, the Save-Limpopo, the Olifants River, and the Lebombo. Dikes of both Jurassic and Proterozoic age have been identified within the ESE-trending Okavango dike swarm (Jourdan *et al.*, 2006), suggesting that the Jurassic events represent the reactivation of a pre-existing trend, and calling into question Jurassic kinematic reconstructions made using these dikes. Many older dike swarms are now dismembered, as in the well-documented Central Atlantic dike swarm of Africa, North and South America (May, 1971). Magnetic identification of dikes relies on simple pattern matching from contour maps generated from simple source geometries (Vacquier *et al.*, 1951). The depth to the top of dikes can be a valuable indicator of the kinematics of post-dike faulting (Modisi *et al.*, 2000). In Modisi *et al.*'s (2000) study, determination of the depth to the tops of dikes was made using Euler's homogeneity equation (see Section 5.06.4.7). Although the magnetic signature AU85 of a dike is usually easy to recognize, little attention has been directed to the important problem of magnetically recognizing dikes of common trend but dissimilar ages from within a single swarm. There are likely to be significant differences in magnetic signature, although the identification and mapping of these differences will require inputs from both field and laboratory studies.

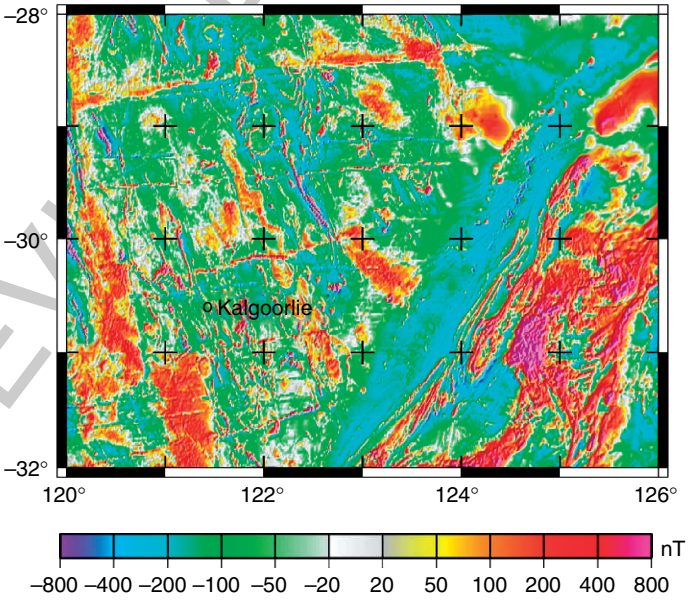

f0010 **Figure 2** Total field anomaly (ΔT) over Australian dikes of the Archean Yilgarn craton. The E-W trending set seen here is part of the Widgiemooltha dike swarm, dated at 2410 Ma. Map based on a 1-km grid rendition of the Magnetic Anomaly Grid AU10 Database of Australia (Milligan, 2005). Artificial illumination from the East and Southeast. The Kalgoorlie gold and precious metal district is located in the central portion of the figure. Many of the ore deposits in this district are localized along fractures and shear zones (Weinberg *et al.*, 2004). Mercator projection.

s0060 ### 5.06.3.3 Cenozoic–Recent Faulting in Forearc Basins

p0130 Forearc basins around the Pacific Rim are the site of devastating earthquakes because of their proximity to large population centers. Three types of earthquakes (mega thrust contact, deep intra-slab, and shallow) are commonly encountered in these basins (b1515 Saltus *et al.*, 2005). The faults that host earthquakes occurring along shallow crustal faults in the overriding continental plate can sometimes be located with high-resolution magnetic surveys. The Seattle fault zone, an east-trending zone of reverse faulting extending through Seattle, Washington, was the site of an M7 earthquake about 1100 years ago (b0195 Bucknam *et al.*, 1992), and is an example of such a fault. Mapped geologically and with an aeromagnetic survey (b0170 Blakely *et al.*, 2002), and studied along several profiles with seismic reflection surveys, this region hosts a tripartite package of rocks in close proximity to the fault zone. The package has a distinct magnetic signature, and allows the fault zone to be traced in areas of poor exposure, or where it is covered. From north to south, the package consists of a magnetic Miocene volcanic conglomerate, a thick sequence of nonmagnetic marine and fluvial rocks, and variably magnetic volcanic and sedimentary rocks of Eocene age. After accounting for remanent magnetization, the magnetic contacts were picked objectively (b0160 Blakely and Simpson, 1986). Near-surface features of this magnetic survey have also been enhanced using a matched filter approach (b1630 Syberg, 1972; b1250 Phillips, AU86 1997; and see Section 5.06.5.5.2.(ii)). The deformation front of the Seattle fault zone, as revealed by the seismic reflection data, lies immediately north of, and locally coincident with, the magnetic conglomerate. The aeromagnetic survey can also provide information on individual strands of the fault zone, and whether it is segmented (b0170 Blakely *et al.*, 2002). The longer wavelength information within these aeromagnetic surveys (b0390 Finn, 1990; b0140 Blakely *et al.*, 2005, b1770 Wells *et al.*, 1998) can be used to provide a regional context for the tectonics of the Cascadia forearc region that hosts these basins.

s0065 ### 5.06.3.4 Heat Flux Beneath the Antarctic Ice Sheet

p0135 Using magnetic data to infer heat flux is possible because the magnetic properties of rocks are temperature dependent, and at the Curie temperature rocks lose their magnetism. The geothermal heat flux is an important factor in the dynamics of ice sheets, the occurrence of subglacial lakes and onset of ice streams, and may affect the mass balance. Direct heat flux measurements in ice-covered regions are difficult; thus, b0395 Fox Maule *et al.* (2005) developed a method using first-order features of the satellite magnetic data to estimate the heat flux underneath the Antarctic ice sheet. They found that it varies from 40 to 185 mW m^{-2}, that areas of high heat flux coincide in part with known current volcanism, subglacial lakes, and ice streams, and that some areas landward of the Ronne ice shelf near the shoulder of the West Antarctic rift system may host active, but undiscovered, subice volcanic regions.

p0140 Traditional methods for inferring heat flux, or the related magnetic problem of inferring the bottom of the magnetic crust, have relied on the shape of radially averaged spectra from gridded aeromagnetic data sets (b1610 Spector and Grant, 1970; b0940 Maus *et al.*, 1997). To quote Blakely (1995), "this calculation ranks AU11 among the most difficult in potential field inversion." At all wavelengths, the contribution from the bottom of the magnetic source is dominated by contributions from the top. The top of the source must be also be known, in itself a difficult problem. The estimate of the bottom focuses on the lowest wave numbers, which overlap with poorly known regional fields that may be unrelated to bottom of the magnetic bodies. There also exists a dependence on the characteristic shape of the magnetic bodies, and an assumption about the magnetization distribution. Assuming the magnetization is spatially uncorrelated ('white') is common, although magnetic susceptibility distributions are often correlated (b1285 Pilkington and Todoeschuk, 1995).

p0145 The method of b0395 Fox Maule *et al.* (2005) uses a self-consistent compositional and thermal model of the mantle and crust (b1095 Nataf and Ricard, 1996) as a starting point, and this model is then modified in an iterative fashion with the satellite data until the magnetic field predicted by the model matches the observed magnetic field. At the scale of the surveys used (400+ km wavelength), a unique solution is guaranteed by assuming that induced magnetizations dominate over remanent magnetizations in continental crust, and that vertical crustal thickness variations dominate over lateral susceptibility variations (b1330 Purucker and Ishihara, 2005). The resulting magnetic crustal thickness is then used as one boundary condition in a thermal model of the continental crust, assuming one-dimensional (1-D) heat conduction, and using a simple model to account for radioactive

heat production in the crust. The largest complications and uncertainties in this approach are (1) uncertainties in determining the magnetic field model in the dynamic, high-latitude auroral, subauroral, and polar cap region, (2) the starting seismic and thermal model, (3) uncertainties in the upper and lower temperature boundary conditions, (4) lateral variations in thermal conductivity, and (5) lateral variations in viscous remanent magnetization.

5.06.3.5 Northern Canadian Kimberlite Province

Diamond-bearing kimberlites were first recognized in rocks of cratonic North America more than 150 years ago. Exploration interest focused on the Slave Craton in Canada beginning in the 1970s, and the discovery of diamond-bearing kimberlites in the early 1990s set off a mineral staking rush (Krajick, 2001). By 2004 these deposits accounted for 15% of global diamond output by value. The exploration program relied on a complementary suite of geochemical and geophysical techniques, of which the magnetic technique was one. Exploration usually proceeded from a program of indicator mineral sampling, to one of geophysical surveys in favorable regions, and finally to drilling in order to prove the deposits (Power *et al.*, 2004). Airborne total magnetic field and electromagnetic surveys, and follow-up ground surveys, were the most common geophysical surveys performed (Jansen and Witherly, 2004), although sometimes gravity, ground-penetrating radar, and seismic techniques were used. The kimberlite host rock often exhibits a positive magnetic susceptibility contrast, and a strong remanence, compared to the surrounding country rock, commonly a high-grade metamorphic rock, or granite, in the Slave Craton. Kimberlite pipes are often found in geographically localized groups, frequently under lakes because of differential erosion, and the remanence directions within those groups is often similar. Kimberlite pipes are often associated with diabase dikes (see previous section for a discussion of their magnetic signature), and are also commonly intruded along pre-existing zones of weakness (regional faults, geological contacts), many of which will have magnetic signatures. A completely preserved kimberlite pipe may be several hundred meters wide, and is often pipe- or carrot-shaped (Macnae, 1979). The resulting magnetic anomalies are usually circular in form (because the area is near the magnetic pole; see Section 5.06.5.4.2), and data enhancement techniques are similar to those used for impact craters (see Section 5.06.3.1). The use of the analytic signal (see Section 5.06.4.6), and a pattern-recognition technique (Keating and Sailac, 2004), has been shown to be of some use in identifying possible kimberlite target rocks.

5.06.3.6 Structural Control of the Urengoy Gas Field

The West Siberian Basin, one of the world's largest sedimentary basins developed on continental crust, hosts a supergiant gas accumulation in the Urengoy field (Littke *et al.*, 1999). The hydrocarbons in the Urengoy are found in an anticlinal trap defined by rejuvenated graben faults (Gibson, 1998; Grace and Hart, 1990). Aeromagnetic (Makarova, 1974) and gravity (Arctic Gravity Project, 2002) mapping (**Figure 3**) over this region reveals north–south-trending positive anomalies that are fundamentally lithologic, originating in Permo-Triassic basalt now found in rift basins. The basalt in these buried grabens is of the same age (Reichow *et al.*, 2002) as the bulk of the Siberian traps exposed further east on the Siberian platform.

The Siberian traps, part of the largest recorded terrestrial flood basalt province, is contemporaneous with the end-Permian extinction (Erwin, 1994), the largest mass extinction of the Phanerozoic, although a causal relation between the two has not yet been established (Elkins-Tanton and Bowring, 2006). The West Siberian rift basins define the base of the sedimentary column, and subsequent post-rift deposition from the Jurassic to the Cretaceous consists of fluviatile and marginal marine sediments. The boundary faults of these basins were reactivated later, and hence the magnetic and gravity anomalies serve to reveal indirectly the faults that define the hydrocarbon trap. The graben faults were rejuvenated in the Early Cretaceous, and created broad arches in the Cretaceous sediments. Maturation of Jurassic source rocks was followed by migration of hydrocarbons into traps located within the Pokur Formation of Cenomanian age.

5.06.4 Compilations and Models

Because maps of the crustal magnetic field are so useful for regional geologic understanding, and because magnetic surveys are usually acquired over small regions, there is a need to assemble the individual magnetic

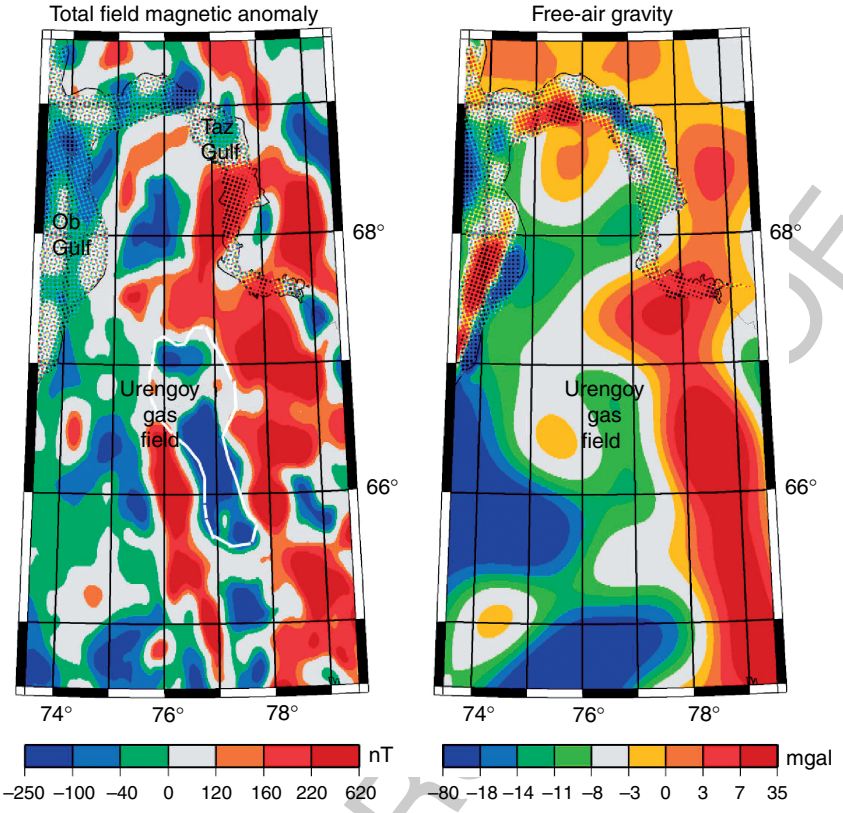

f0015 **Figure 3** Aeromagnetic total field anomaly (ΔT) and free-air gravity maps of a portion of the West Siberian Basin showing the correspondence of magnetic and gravity lows with the Urengoy gas field. This coincidence is a consequence of both lithologic and structural factors (Gibson, 1998). The magnetic data are extracted from compilations of Makarova (1974), and Geol. Sur. Canada (1995), the gravity data come from the Arctic Gravity Project (2002), and the field boundaries of the Urengoy field are from Grace and Hart (1990). Lambert projection.

surveys into larger compilations. This assembly is often assisted by the addition of longer, higher-altitude magnetic surveys that serve to tie the individual surveys together, and ameliorate the discontinuities that occur at survey boundaries. Perhaps the best known of these higher-altitude surveys are a series of surveys flown in Australia (Tarlowski *et al.*, 1996) for the purpose of leveling the Australian magnetic map, and the Project Magnet surveys (Coleman, 1992) of the US military. In North America, the 1970s saw the first regional compilations, followed by partial compilations of the entire continent in the 1980s, and more complete compilations by 2003. Similar scenarios have played out in Australia, the Former Soviet Union, China, South Asia, Australia, the Arctic and Antarctic, in Europe, and over the world's oceans. In contrast, Africa and South America are less advanced in terms of magnetic compilations, most of which have been led by industrial consortiums. The longest wavelengths of the crustal magnetic field can be measured from satellites in near-Earth orbits, and beginning in the 1960s, Russian and US satellites began to measure those magnetic fields. This effort continues today as an international effort, with the CHAMP satellite, and the upcoming ESA Swarm mission. Earlier comparisons (Schnetzler *et al.*, 1985) suggested a difference in amplitude between the crustal field measured at or near the surface and from satellites when the data sets were compared at the same altitude, with the satellite amplitude lower, but the two approaches are beginning to converge (e.g., Ravat *et al.*, 2002). Upcoming satellite missions will use a gradiometer configuration to go to spherical harmonic degree 130+, and the wavelength content of near-surface surveys is being enhanced at both ends of the wavelength spectrum. There still remains a gap in our knowledge of magnetic anomalies with wavelengths from about 200 to 400 km. Only in Australia (Ravat *et al.*, 2005) is this gap partially filled. AU13 Community efforts are now focused on the development of a World Digital Magnetic Anomaly Map

(WDMAM), planned for release in 2007 (see Section 5.06.4.2).

p0170 In parallel with the development of compilations has been the development of larger and more elaborate models of the magnetic field, built on a deepening understanding of the sources of the magnetic field. These models utilize both forward and inverse approaches, and are frequently tested, and enhanced, using data from the compilations.

s0085 5.06.4.1 Continental-Scale Compilations

p0175 The first experimental airborne total field magnetometer was flown in the USSR in 1936 (Gibson, b0440 1998) and in 1974, the Ministry of Geology of the USSR published a mosaic series of 18 sheets at 1:2.5 million scale showing the residual magnetic intensity (Makarova, b0905 1974) over the USSR and surrounding waters. These sheets were digitized in 1982 by the US Naval Oceanographic Office, Stennis Space Center Mississippi in order to produce four regional one-arc-minute grids of magnetic anomaly values covering the entire Former Soviet Union. These digital data were provided to the National Geophysical Data Center (NGDC, 1996) for archival and public dissemination. The digitized data were made available on a 2.5-km grid.

p0180 The first continental-scale compilation, of North America (Hinze b0625 *et al.*, 1988), was completed in preliminary form as part of the Decade of North American Geology, and released by the Committee for the Magnetic Anomaly Map of North America in 1987. Consisting of the aeromagnetic surveys of Canada and the US, and surrounding waters, the compilation effort had been preceded by compilations of US (Zietz, b1825 1982) and Canada (Hood b0650 *et al.*, 1985). The North American compilation was released as a 2-km grid. The addition of aeromagnetic surveys over Mexico, and improved Canadian and US maps, led to a second-generation product (Bankey b0060 *et al.*, 2002; Hernandez b0605 *et al.*, 2001). The data grids comprising this map have a variety of wavelength content, 1-km grid spacing, and show the total field at 1 km above the terrain. They are projected using a spherical transverse Mercator with a central meridian of 100° W, base latitude of 0°, scale factor of 0.926, and Earth radius of 6 371 204 m. Wavelengths greater than 150 km are poorly represented in this compilation.

p0185 Magnetic observations of the North Atlantic and Arctic oceans, and adjacent landmasses, were compiled as part of a Geological Survey of Canada program (Macnab *et al.*, 1995; Verhoef b1720 *et al.*, 1996, and **Figure 4**). The final data set, on a 5-km grid, was merged from three subgrids of (1) digital airborne observations, (2) digital shipborne observations, and (3) pre-existing grids or digitized maps. Only the shipborne observations showed some agreement with the satellite measurements of the crustal magnetic field, and as a consequence, all three subgrids were filtered to remove wavelengths greater than 400 km prior to merging.

p0190 European magnetic observations, from northern, western, and eastern Europe, were compiled by Wonik b1805 *et al.* (2001) on a 5-km grid at an altitude of 3 km above mean sea level (**Figure 4**). Long wavelengths were retained in this survey, although comparisons with satellite data suggest that wavelengths in excess of 300 km are poorly resolved. The map is projected using a Lambert Conformal Conic with a central meridian of 20° E, and standard parallels at 30° and 60° N.

p0195 A compilation of magnetic maps of onshore and offshore regions of China, Mongolia, and Russia with accompanying interpretation was produced by a

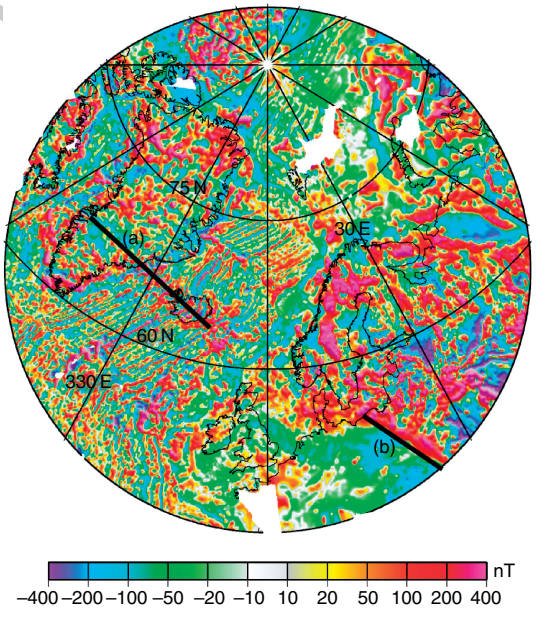

f0020 **Figure 4** Total field anomaly map (ΔT) in a Gnomonic projection showing parts of the merged compilations of Europe (Wonik, 2001) and the North Atlantic/Arctic (Verhoef *et al.*, 1996) for use in the ongoing WDMAM project (Purucker and Mandea, 2005). Straight lines on Gnomonic projections are great circle arcs on the sphere. The surface trace of the Iceland hot spot (a) and the Tornquist-Teisseyre line (b) separating Precambrian from Paleozoic Europe are two examples of such features (Purucker and Whaler, 2003). AU14

team from the Geological Survey of Canada (1995). The data were on a 5-km grid, and wavelengths in excess of 400 km have been removed from the map, which is displayed with a transverse Mercator projection.

p0200 A digital compilation of marine and aeromagnetic data over South Asia (Geol. Sur. Japan, 2002) was produced on a 2-km grid. A Lambert azimuthal equal-area projection was used with a central point at 15° N 120° E, and a terrestrial radius of 6377 km.

p0205 A digital compilation of aeromagnetic data over Australia and the surrounding oceans in now in its fourth edition (b1020 Milligan and Franklin, 2004; b1015 Milligan *et al.*, 2005). The associated database contains publicly available airborne magnetic grid data for onshore and near-offshore Australia. Flight-line magnetic data for each survey have been optimally gridded and the grids matched in one inverse process. Composite grids at 250- and 400-m grid spacing are available. Aeromagnetic traverses flown around Australia during 1990 and 1994 are used in both quality control of the grids they intersect, and also to constrain grid merging by forcing grid data, where intersected, to the level of the traverse data. The map is displayed with a Lambert Conformal Conic Projection.

p0210 A sparse grid of aeromagnetic and marine magnetic data, supplemented by satellite magnetic coverage, is available for the Antarctic (Golynsky *et al.*, 2002). The data set is publicly available as a 5-km grid, referenced to a polar stereographic projection.

p0215 The first compilation of onshore and offshore magnetic anomaly maps for China date from the late- 1980s (Chinese National Aerogeophysics Survey and Remote Sensing Center, 1989), and has been recently (2004) updated in digital form.

p0220 Industry-led consortia have produced magnetic compilations of Africa (b0080 Barritt *et al.*, 1993), Arabia, India, and the Middle East (b1100 Reeves and Erren, 1994), and South America (b0435 Getech, 1996).

p0225 Oceanic data sets (GEODAS, 1999) are held by the National Geophysical Data Center of NOAA. The most recent regional compilations are by b0680 Ishihara (2004) and b1350 Purucker and Ishihara (2005), where the subtraction of non-crustal magnetic field sources was done using the CM4 model of b1500 Sabaka *et al.* (2004) (see Section 5.06.5.2).

s0090 5.06.4.2 WDMAM Compilation

p0230 Although aeromagnetic data have been collected for almost 70 years, no worldwide compilation of them yet exists. An initiative of the International Association of Geomagnetism and Aeronomy has as its goal the production of a 5-km grid of the crustal magnetic field at an altitude of 5 km. The minimum wavelength represented by such a grid will be twice the grid spacing, or 10 km.

p0235 The unveiling is planned for the General Assembly of IUGG/IAGA at Perugia, July 2007 (Korhonen *et al.*, 2005; b1380 Ravat *et al.*, 2003, b1405 Reeves *et al.*, 1998). The map will utilize airborne, marine, and satellite data to capture as many wavelengths as possible between 10 and 2200 km. It will include all freely available major digital national and regional anomaly data sets: Arctic-North Atlantic, North America, Europe, South Asia, North East Asia, Eastern Indian Ocean, Australia, and the Antarctic. It will also include lower-resolution grids extracted from the proprietary coverage of b0435 Getech (1996) for Africa and South America. Getech's web page contains maps showing aeromagnetic coverage worldwide in their holdings. Another view of the worldwide coverage can be seen in b1405 Reeves *et al.* (1998). AU15

s0095 5.06.4.3 Satellite Compilations of Crustal Magnetic Fields

p0240 Satellite models of crustal magnetic fields are commonly SHAs of data gathered during magnetically quiet times, rather than the field data directly. Two current models of this type are MF-4 (b0930 Maus *et al.*, 2006) and CM4 (b1500 Sabaka *et al.*, 2004). The two models reflect somewhat different design philosophies, and hence have different strengths: MF-4 is an inversion of data from which estimates of other magnetic field sources have been removed, whilst CM4 solves for all sources, suitably parameterized, simultaneously. Thus MF-4 is a crustal field model only, and extends from degrees 16 to 90. The CHAMP magnetic field satellite input to MF-4 has had removed an internal field model to degree 15, an external field model of degree 2, and the predicted signatures from eight main ocean tidal components. Additional external fields are subsequently removed in a track-by-track scheme. Because of its design philosophy, the MF-4 model can be considered a minimum estimate of the crustal magnetic field, one in which there will be some suppression of along-track magnetic fields. Regularization has been applied to degrees higher than 60 to extract clusters of spherical harmonic coefficients that are well-resolved by the data.

p0245 CM4, in contrast, is a comprehensive model, that is, it includes components of internal and external origin, and toroidal fields, in addition to the crustal

field (**Figure 5**). It is based on data from all high-precision satellite magnetic field missions, beginning with the POGO missions of the 1960s. It uses an iteratively reweighted least-squares approach to solve for all of the 25000+ parameters using more than 2 million observations. Because of its design

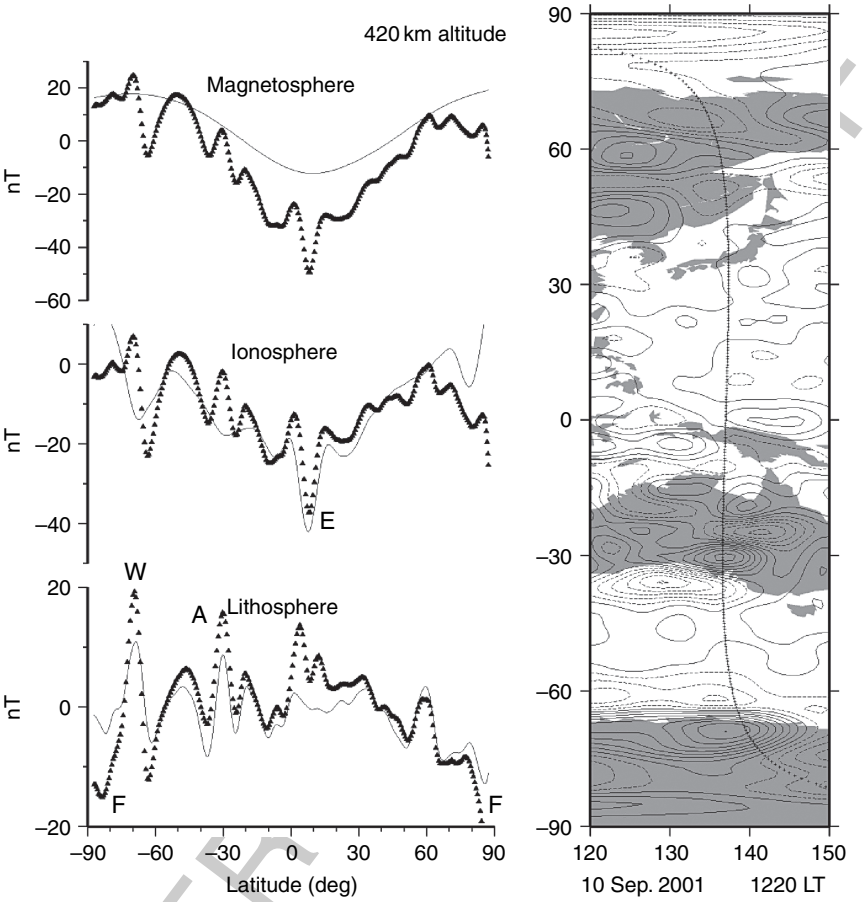

f0025 **Figure 5** Residual progression versus geographic latitude as magnetic fields from the four main source regions (core, crust, ionosphere, and magnetosphere) are removed with the Comprehensive Model CM4 (Sabaka *et al.*, 2004). This profile shows the total field *T* in the direction of the main field **F** of a CHAMP descending (South-going) satellite pass on 10 September 2001. The pass is centered at 0300 UT and crosses the Equator at 137° W and 1220 LT. Magnetically quiet conditions prevailed with $Kp = 1^+$ for this period, $Kp = 0^+$ for the previous 3-h period, $Dst = 2$ nT, and $|d(Dst)/dt| < 2$ nT h^{-1}. Siebert and Meyer (1996) discuss magnetic indices, while Mandea and Purucker (2005) discuss their role in data selection (see also appendix to Chapter 3). For a given panel, the symbols represent residuals with respect to a main field (to spherical harmonic degree 13) plus all fields labeled in the panels above; the line is the prediction from the field source labeled in the current panel. The figure on the right shows the location of the sub satellite point and includes a contour map of the total field anomaly (ΔT) originating in the crust (to spherical harmonic degree 60) from the Comprehensive Model (contour interval = 2 nT, dashed lines indicated negative ΔT). The data from this profile were not included in the construction of the Comprehensive Model. The equatorial electrojet (EE) can be seen (E) because it is most prominent around mid-day, following the magnetic dip equator. Although the amplitude of the EE in the model and profile is similar, a slight amplitude offset and latitudinal shift results in a residual anomaly that might be mistaken for a crustal anomaly. While the EE is a robust feature of the low-latitude ionosphere, it does exhibit significant variability on a day to day basis (Lühr *et al.*, 2004; Langel *et al.*, 1993), and includes wavelengths shorter than the resolution of CM4 (spherical harmonic degree 45 for the EE). The magnetic field originating in the distant magnetosphere exhibits variations, which are not entirely accounted for by the Dst index, and this may account for some of the mismatch. In contrast, the high-latitude current system (F) exhibits significant variability in time on a minute-to-minute basis, and in space, and CM4 does not attempt to model it. Two significant crustal anomalies, in Wilkes Land, Antarctica (W), and in southern Australia (A) are prominent in the profile. The frequency content of these anomalies again exceeds the cutoff of CM4 (spherical harmonic degree 65 for crustal fields). These two magnetic features (Purucker *et al.*, 1999; Mayhew and Johnson, 1987) were adjacent (Von Frese *et al.*, 1986) in pre-rift reconstructions of Gondwana.

philosophy, the CM4 crustal field component estimate is expected to have more power than MF-4, both because no direct damping is applied to the crustal field coefficients, and because of the along-track approach used by MF-4. No suppression of along-track magnetic fields is expected, and some of them, especially in the vicinity of the dip equator, are of questionable crustal origin.

s0100 5.06.4.4 Global Magnetization Models

p0250 Global magnetization models often represent an integration of compositional and thermal models of the crust and mantle with long-wavelength crustal magnetic field measurements from satellite. Both forward (b0595 Hemant and Maus, 2006) and inverse (b0395 Fox Maule *et al.*, 2005) approaches are currently under development. For example, one approach (b1540 Purucker *et al.*, 2002) has used the 3SMAC (b1095 Nataf and Ricard, 1996) compositional and thermal model of the crust and mantle as a starting model, which is then modified in an iterative fashion with the satellite data until the magnetic field predicted by the model (**Figure 6**) matches the observed magnetic field. A unique magnetic crustal thickness solution is obtained by assuming (1) that induced magnetizations dominate in continental crust, (2) the model of b0355 Dyment and Arkani-Hamed (1999) describes the

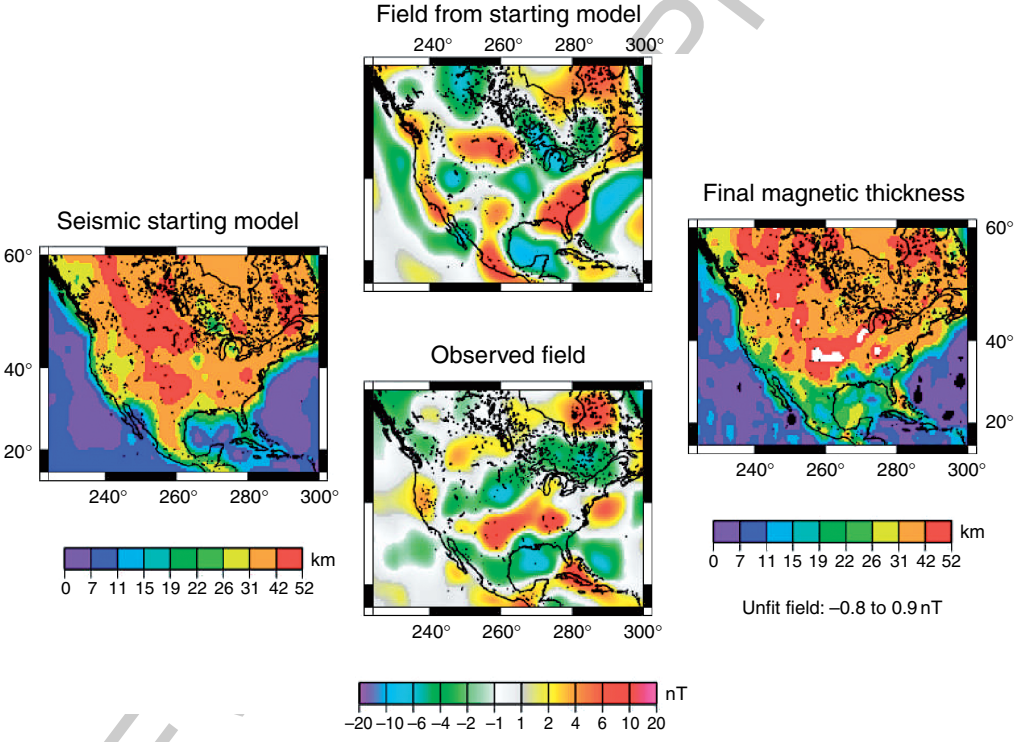

f0030 **Figure 6** Magnetic crustal thickness map of North America (right), which reproduces satellite observations (bottom) from CHAMP, as represented by MF-4 (Maus *et al.*, 2006). As a starting model the seismic crustal thicknesses (left) from Chulick and Mooney (2002) over North America are used instead of the global 3SMAC crustal and thermal model (Nataf and Ricard, 1996). The magnetic field is calculated from this starting model (top) under the assumption of a constant magnetic susceptibility (χ) of 0.04, and long-wavelength fields (spherical harmonic degree < 15) are removed, simulating a main field subtraction. The observed (bottom) and modeled (top) fields are differenced, and the difference is inverted for a magnetic crustal thickness. The starting model is then updated to reflect this change, and the process continues until convergence is achieved. The process is nonlinear because the total anomaly field (ΔT) is used, and because of the high-pass filter. After three iterations of this technique the residuals to the observations are less than ± 1 nT. Negative magnetic crustal thickness (shown in black, the minimum is -6 km) over a few regions in the ocean could be a consequence of remanent magnetic fields. Large magnetic crustal thicknesses (shown in white; the maximum is 60 km) over parts of the mid-continent region could be a consequence of inaccuracies in the starting model. b1340 Purucker *et al.* (2002) applied this approach over North America, and found that if 3SMAC alone was used as a starting model, negative crustal thicknesses were found over the southeastern US landmass. Modification of 3SMAC to place the major crustal thickness change near the Coastal Plain/Piedmont boundary resulted in more realistic crustal thicknesses.

oceanic remanence, and (3) that vertical thickness variations dominate over lateral susceptibility variations. A starting model is necessary for two reasons: (1) to constrain wavelengths obscured by overlap with the core field, and (2) to ensure that most magnetic crustal thicknesses will be non-negative. An approach (**Figure 6**) such as this has been used to define the thickness and thermal properties of cratonic North America (Purucker[b1340] *et al.*, 2002).

p0255 A second approach (Hemant[b0595] and Maus, 2006; based on earlier work of Hahn[b0540] and Bosum, 1986) uses the available magnetic petrology, geological age, tectonic and seismic crustal thickness information of the Earth's crust, and assigns magnetization strengths and directions to geological units based on their age and rock compositions. In this way a global magnetization model of the Earth's crust is computed. The model is used to predict the crustal magnetic field at satellite altitude and compared with the observed crustal field measurements. One can match the observed field by varying the boundaries and composition of lower-crustal structures.

s0105 5.06.5 The 'Tools of the Trade'

s0110 5.06.5.1 Survey Design and Resolution

p0260 Although magnetic surveys are frequently conducted as 'missions of opportunity', where the mission design is largely dictated by the needs of the primary instrument, or the platform, there are many cases in which the collection of a magnetic survey is the primary goal, and consideration needs to be given to optimizing the return from the survey. A recent example of such a process, and its documentation, has been the planning for the Swarm magnetic field satellite constellation (Olsen[b1130] *et al.*, 2006b). Survey design of aeromagnetic surveys, including the spacing of flight lines, their altitude, and the inclusion of tie lines, is discussed by Reid[b1420] (1980). For further details, refer 00089 on Observation techniques.

s0115 5.06.5.2 Removal of Noncrustal Fields

p0265 An important part of obtaining crustal anomalies suitable for further processing, modeling, and interpretation is adequate removal of noncrustal fields, primarily that arising from dynamo action in the core, and external fields due to solar–terrestrial interactions. The geodynamo-generated field, often referred to as the main field, has large amplitude but varies slowly, both temporally and spatially. External fields have much smaller amplitudes but have much more rapid temporal and spatial variations. Time-varying external fields also induce subsurface magnetic fields throughout the crust and mantle, but their amplitudes are generally small compared to those of typical crustal anomalies.

p0270 The effect of external fields can be minimized by collecting data at magnetically quiet times, but this is frequently impractical, especially at higher magnetic latitudes. Many surveys are conducted with a continuously recording base station to monitor and correct for external variations. The base station is located at a site where the spatial field gradients are low (i.e., not on a magnetic anomaly), ideally in, roughly, the center of the survey area. It can be used to alert surveyors to magnetic storms, when data acquisition will be suspended, and as a means to judge the quality of the survey data. In periods of normal activity, the temporal variations recorded at the base station will be a reasonable approximation to the external field throughout the survey area. External fields are a minimum at night in low and mid-latitudes. Over several days (or longer) it is usually possible to identify a 'night time quiet value' (NTQV) from the base station record. The difference between the NTQV and the base station value at a given time is an approximation to the external field at that time, and is removed from the survey data. The difficulty of this method lies in the complicated behavior of the external field, combined with the generally unknown conductivity structure of the Earth. A second approach to the correction of external fields is via a least-squares analysis of the misties at intersecting survey lines (Ray[b1390], 1985). The two approaches are often used together, with the regression-type analysis used as a refinement, to remove errors not removed by the first approach.

p0275 After correcting for external fields, the method for removing the main field depends on the size and scope of the survey. For a small, ground-based survey, it is often sufficient to treat the main field as constant over the survey area. Its amplitude is likely to be well-approximated by the average field (data mean) or the NTQV. Airborne and satellite surveys typically cover much larger areas, over which it may not be reasonable to assume the main field is constant, and therefore more sophisticated main field removal methods are justified. An obvious extension is to remove the best-fitting line (for a 1-D survey) or plane (2-D survey) through the data. More commonly, the predictions of a main field model such as the International Geomagnetic Reference Field

(IGRF) are subtracted. IGRFs consist of values for the spherical harmonic coefficients from which the field can be calculated at any point in space and time (see Chapter 2 for further details). Each IGRF consists of a set of main field and secular variation coefficients covering a 5-year interval, thereby accounting for the temporal evolution of the main field. However, mismatches can occur between crustal anomaly fields in overlapping or abutting areas obtained from surveys at different times because the IGRF representations are not perfect. This is a particular problem when trying to merge surveys to form larger compilations.

The most important data for IGRF modeling have been permanent magnetic observatory night-time values on magnetically quiet days, usually selected on the basis of geomagnetic activity indices (see the Appendix to Chapter 3, and Siebert[b1565] and Meyer, 1996). Observatories are located in areas of low spatial magnetic field gradients, in areas where crustal fields are a minimum. With the incorporation of large numbers of data from orbiting satellites, and the availability of more powerful computational resources, different methods of analysis become appropriate. As described earlier, rather than attempting to remove certain field sources from the data on a point by point basis prior to main field modeling, they can now be solved for simultaneously. This approach has led to the series of 'comprehensive models' (e.g., Sabaka[b1500] *et al.*, 2004) in which large numbers of parameters expressing the main, crustal, external, and induced fields are co-estimated (see Chapter 2). These models (**Figure 7**) should enable better estimates of the crustal field to be obtained from survey data (Nabighian[b1070] *et al.*, 2005). The current version of the 'comprehensive model' is CM4 (Sabaka[b1500] *et al.*, 2004) and the data envelope extends from 1960 through July of 2002. Usage of the model outside of this time range entails two steps. First, the user must update the values of Dst and F10.7, the indices used for characterizing the state of the ionosphere and magnetosphere. Second, the internal, time-varying low-degree part of the model must be replaced by a model that is valid over the time span considered. This would mean the IGRF for data collected prior to 1960, and a model such as the CHAOS model (Olsen[b1125] *et al.*, 2006a) for data collected after July 2002. The end result of this data-reduction process should be point representations of our best estimates of the crustal magnetic field, often referred to as the crustal anomaly field.

5.06.5.3 Representations

Taking the cue from the way seismic trace information is displayed, crustal magnetic data collected along a profile, or even a series of profiles, can be represented as a set of 'wiggles', with areas above the zero line filled, or the areas above and below the line colored differently. More often, data collected over an area are interpolated onto a regular grid for display as a color image, and for further processing and modeling. Various algorithms are suitable for gridding crustal magnetic data, and which is employed in a particular instance will depend on how the data have been collected, and the form of the crustal anomalies encountered. For example, aeromagnetic data usually have a much smaller interval between data points along flight lines than between them (see Chapter 4), making bidirectional spline gridding (Bhattacharyya[b0105], 1969) appropriate. For more evenly spaced data, minimum curvature methods (Smith[b1595] and Wessel, 1990) are often applied. Widely spaced tie lines are often flown perpendicular to the survey direction, and this facilitates the 'leveling' of the survey (Ray[b1390], 1985). If the anomalies have a particular directionality to them (e.g., they arise from a series of parallel dykes), interpolations of the crustal anomaly field can be improved by incorporating measured horizontal gradients (Reford[b1410], 2006). Besides offering a visual image of the data through imaging, these regular grids form the basis for all the transformations (mostly using wave-number domain manipulation) discussed below that can be applied to the data. As a consequence this is an area of continuing research (O'Connell[b1120] *et al.*, 2005; Hansen[b0550], 1993; Cordell[b0290], 1992; Keating[b0740], 1993; Ridsdill-Smith and Dentith[b1455], 1999).

There are many methods of modeling the data that can be used to interpolate between data points and extrapolate beyond the survey area. Some of these are only useful for local modeling, others are only applicable to data sets covering all, or at least a large part of, the Earth's surface, and some can be used for both local and global modeling. Global methods are well-summarized in Langel[b0805] and Hinze's 1998 book, and they present the methods outlined below in a uniform notation.

The most commonly employed global method is SHA, which has been described in chapter 2 in the context of main field modeling. The potential is expressed as

$$V = a\sum_{n=1}^{N_{\max}}\left(\frac{a}{r}\right)^{n+1}\sum_{m=0}^{n}\left(g_n^m\cos(m\phi) + h_n^m\sin(m\phi)\right)P_n^m(\cos\theta) \quad [6]$$

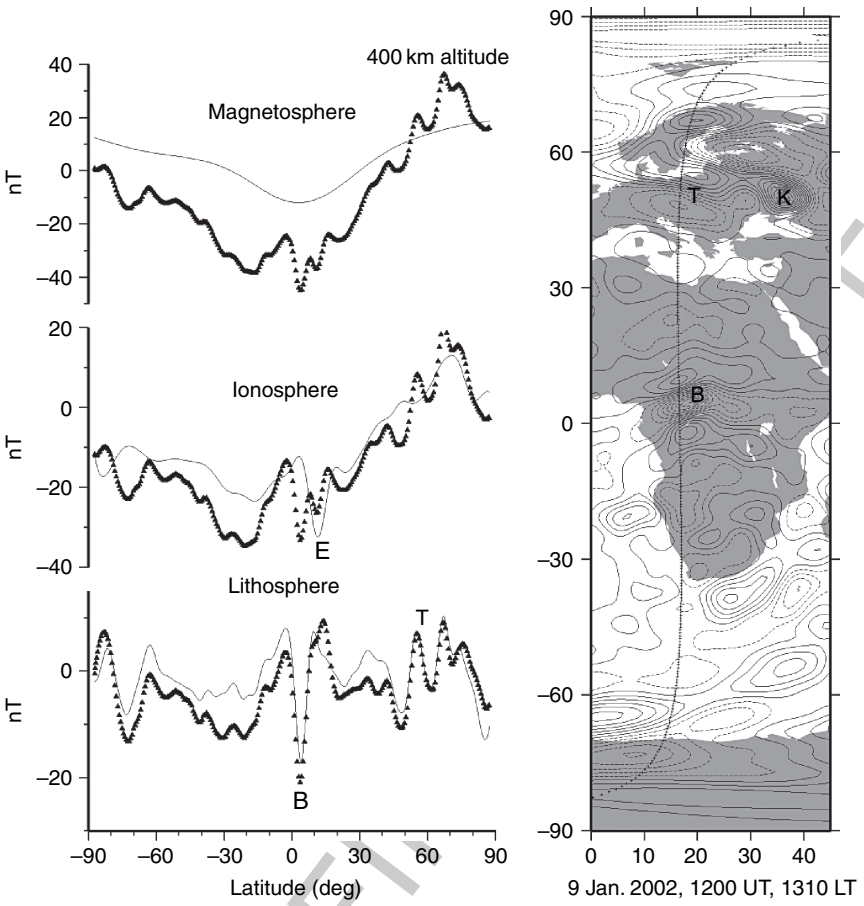

f0035 **Figure 7** Residual progression versus geographic latitude as magnetic fields from the four main source regions (core, crust, ionosphere, and magnetosphere) are removed with the Comprehensive Model CM4 (Sabaka *et al.*, 2004). This profile shows the total field *T* in the direction of the main field **F** of a CHAMP satellite pass on 9 January 2002, when the magnetic field was in a quiet state. The data from this profile were not included in the construction of the Comprehensive Model. For a given panel, the symbols represent residuals with respect to a main field (to spherical harmonic degree 13) plus all fields labeled in the panels above; the line is the prediction from the field source labeled in the current panel. The figure on the right shows the location of the sub satellite point and includes a contour map of the total field anomaly (ΔT) originating in the crust (to spherical harmonic degree 60) from the Comprehensive Model (contour interval = 2 nT; dashed lines indicate negative ΔT). This figure illustrates the ionospheric/lithospheric separation that is possible with a Comprehensive Model approach with the equatorial electrojet (E) in close proximity to the Bangui (B) crustal anomaly (Girdler *et al.*, 1992). Note also the Tornquist-Teisseyre zone (Taylor and Ravat, 1995) (T), a major litho-tectonic structure in Central Europe, and the Kursk (Taylor and Frawley, 1986) anomaly (K), associated with a substantial Banded Iron Formation.

where a is the radius of the Earth, r is the radial distance of the observation from the center of the Earth, ϕ denotes longitude, and θ co-latitude, $P_n^m(\cos\theta)$ are the Schmidt quasi-normalized associated Legendre functions of degree n and order m, and the g_n^m and h_n^m are the spherical harmonic coefficients to be estimated. The difference for crustal field modeling is that the series needs to include much higher harmonic degree terms ($N_{\max}$) to represent the anomaly field adequately. Spherical harmonic models of the crustal field from satellite data (Sabaka *et al.*, 2004; Maus *et al.*, 2006) now go to spherical harmonic degrees as high as $N_{\max} = 90$, corresponding to $N_{\max}(N_{\max}+2)$ coefficients. This creates computational difficulties (Cain *et al.*, 1989; Lesur and Gubbins, 1999), and high-resolution data sets require enormous numbers of spherical harmonic coefficients to represent them adequately. SHA is not particularly well-suited to global (or near-global) data sets of varying spatial density: since the basis functions are themselves global, the spherical harmonic series must extend up to the degree representing the shortest spatial wavelength in the data set (approximately c/n, where c is circumference, and n is spherical

harmonic degree). The coefficients multiplying these degree terms will not be well-constrained if only a limited area of the globe has coverage at the spatial sampling rate appropriate to determine them and, unless regularization is applied, their numerical values may generate ringing over other parts of the globe. Basis functions with more local support, such as harmonic splines (HS) (Shure *et al.*, 1982), or wavelet-like functions (Lesur and Maus, 2006) are better suited to data sets with variable resolution over the globe.

p0300 Spectral analysis can be applied to data collected along profiles or on a plane, with the usual techniques to avoid ringing, edge effects, and spectral leakage (Parker and O'Brien, 1997; Lowe *et al.*, 2001). This allows high-resolution data sets to be represented by small numbers of model parameters. Alldredge (1981) introduced rectangular harmonic analysis, suitable when the area covered is small enough for the flat Earth approximation to be appropriate. The method is based on the solution to Laplace's equation in a Cartesian geometry. The data are first transformed into the local Cartesian coordinate system with origin at the center of the region, and then the coefficients are determined. They can be used to predict the field at any altitude, and can also be transformed back to a spherical Earth coordinate system. Malin *et al.* (1996) introduced extra coefficients to remove trends. In an analysis of main field data, they concluded the method was only suitable for interpolation, and not for extrapolation. Nakagawa and Yukutake (1985) used a cosine function weight near the edges of the region subject to rectangular harmonic analysis to reduce edge effects.

p0305 Alldredge (1982) introduced the related concept of cylindrical harmonic analysis, where the equation to be solved is Laplace's equation in cylindrical polar coordinates. He advocated this when the observations displayed cylindrical symmetry. Again, the size of the area to be modeled and single-valuedness of the potential imposes constraints on the arguments.

p0310 A representation useful for both local and global modeling (typically in a Cartesian and spherical coordinate system, respectively), is equivalent source (ES) dipoles, where again the basis support is local. The magnetized crust is divided into blocks, each of which is assumed to have a magnetic dipole at its center. In this case the potential can be expressed as

$$V = -\mathbf{M} \cdot \nabla \frac{1}{d} \qquad [7]$$

where d is the distance between the dipole and the observation location, and $\mathbf{M}$ is the dipole moment. The conversion factor, $\mu_0/4\pi$, between SI and CGS units (cf. Blakely, 1995, p. 67) is implicitly assumed to be included within eqn [7] and subsequent equations relating the potential V to the magnetization **M.** The model parameters of [7] are the direction and magnetization strength of the dipoles. However, magnetization is often assumed to be purely induced, meaning that the dipole directions are known (parallel to the main field); the problem of inferring strength from vector component anomaly data is then linear. The dipoles can be arranged with variable density according to the data distribution, retaining the resolution of the original data set. This can be a far more efficient (i.e., fewer parameter) modeling method than SHA when the spatial resolution of the data set is uneven. Although the distribution of magnetization in the crust reproducing the anomaly data is highly nonunique (Runcorn, 1975; see Section 5.06.5.6), it can be interpreted geologically, especially if *a priori* information has been incorporated in the modeling, whether forward or inverse (see Section 5.06.5.5). ES dipole models (Dyment and Arkani-Hamed, 1998) are widely used for forward modeling since they are intuitively accessible. They can be used straightforwardly to predict the magnetic field at any altitude on or above the Earth's surface, so also provide an excellent tool for upward and downward (analytic) continuation (see Section 5.06.5.4).

p0315 The crustal anomaly field at or above the Earth's surface, even as high as typical orbiting satellite altitudes of a few hundred kilometers, depends on the magnetization of only a small volume of the crust directly beneath the observation point – the footprint of an anomaly measurement is small. Thus when a local basis is used to represent the anomaly field, the matrix relating observations to model parameters is sparse. Using numerical methods for solving sparse matrix systems then allows a large number of basis functions to be included, meaning that the resolution of the original data set can be retained. An application of this to crustal anomaly modeling was by Purucker *et al.* (1996), who applied the iterative conjugate gradient algorithm to ES dipole modeling of a satellite crustal anomaly data set.

p0320 Although nonphysical and therefore not suitable as an interpretation tool, crustal anomaly data can be represented by a subsurface distribution of magnetic monopole sources (O'Brien and Parker, 1993). The AU21 number and positions of the monopoles on the source

sphere are chosen to provide a good representation of the data (again, a spatially variable monopole density can be used to represent spatially variable resolution of the original data); the model parameters are then simply the monopole amplitudes (no assumptions concerning directionality are required).

p0325 The potential is expressed as a sum of potential sources $\varphi_k(\mathbf{r})$, $k = 1, \ldots, K$

$$V(\mathbf{r}) = \sum_{k=1}^{K} \alpha_k \varphi_k(\mathbf{r}) \quad [8]$$

where α_k are the monopole amplitudes to be determined. Monopoles at locations $\mathbf{s}_k$ are represented by functions

$$\varphi_k(\mathbf{r}) = \frac{1}{|\mathbf{r} - \mathbf{s}_k|} \quad [9]$$

The solution is calculated by minimizing

$$U = \left|\left|\mathbf{C}^{-1}(\mathbf{d} - \mathbf{G}\alpha)\right|\right|^2 + \lambda \boldsymbol{\alpha}^T \Gamma \boldsymbol{\alpha} \quad [10]$$

where $\mathbf{C}$ is the data covariance matrix, $\mathbf{d}$ is the data vector, $\mathbf{G}$ is the matrix of Green's functions relating the monopoles to the measurements, λ is a Lagrange multiplier, and $\boldsymbol{\alpha}^T \Gamma \boldsymbol{\alpha}$ is a quadratic form expressing the field complexity. $||\cdot||$ denotes the Euclidean norm or length. $\boldsymbol{\Gamma}$ is known as the Gram matrix; its (j, k)th element is the inner product of φ_j and φ_k. Thus the first term measures the fit to the data, and the second, the amount of structure in the resulting field model. This is an example of a regularized, or minimum norm, solution; by an appropriate choice of λ, we can relax slightly the fit to the model such that it does not attempt to model noise in the data. The quadratic form (and definition of the inner product for the calculation of the Gram matrix) is chosen to measure some global property of the field such as its mean strength or lateral variability; useful measures lead to closed form, or at least easily calculable, Gram matrix elements. The concept was introduced AU22 with main field modeling in mind (see chapter 2), where some quantities that are expressible as quadratic norms can be bounded theoretically or empirically. It is now widely used as a regularizing tool. For crustal modeling, it ensures that the models have minimum structure for a given fit to the data; if the fit is acceptable, we can then argue that the real Earth has at least as much structure as the model. Since [10] minimizes a global measure of complexity, it does not matter if the monopole sources are distributed unevenly over the surface to reflect the data coverage.

HS are local basis functions introduced by Shure[b1560] p0330 *et al.* (1982) for global main field modeling. They were the first to apply minimum norm modeling to geomagnetism. Using the Green's function for the magnetostatic potential, the solution is constructed as a linear combination of the HS associated with each data point, leading to the solution of a linear system of dimension: the number of data points. This is impractically large even for main field modeling, but naturally preserves the resolution of the original data set. To make the inversion of large data sets computationally tractable, Parker and Shure[b1195] (1982) expanded the solution in terms of HS at only a subset of the data points, known as the depleted basis. The system then reduces to one of the dimensions of the number of data points. Tests based on small data sets demonstrated that the depleted basis solution had only a slightly larger norm than the minimum value obtained by HS. The resolution of the depleted basis solution depends on the spacing between the basis points. The field can be constructed at any radius beyond which the solution converges, making analytic continuation straightforward.

HS is not used in crustal anomaly modeling p0335 because the number of points in practical data sets is too large, but Whaler[b1785] (1994) inverted a $2^\circ \times 2^\circ$ grid of MAGSAT satellite crustal anomalies using depleted basis HS, using it to downward continue the field from satellite altitude to just above the Earth's surface. With the computational resources available then, she was only able to retain every other basis point in latitude and longitude even over a continental-sized area of the globe (an $80^\circ \times 80^\circ$ area centered on Africa), with consequent loss of resolution. She also found that a sparse distribution of points was required over the remainder of the globe to avoid ringing. Another disadvantage of depleted basis HS is that the arrangement of depleted basis points is subjective. However, it simplifies the inversion of total field anomaly data, since the basis functions for their expansion can be chosen to be those for the vertical component (at a limited subset of the actual data points), simplifying the matrix element calculations (Langel and Whaler, 1996). AU23

A more satisfactory application of HS uses sparse p0340 matrix techniques, allowing the full basis to be retained. Unpublished models using the conjugate gradient algorithm based on satellite anomaly data are very similar to those obtained using other global methods, and also compare favorably with Whaler's[b1785] (1994) depleted basis models over Africa. HS (and depleted basis HS) coefficients can be converted into

an infinite series of spherical harmonic coefficients that give power spectra similar to those obtained from SHA at low degree, but typically have less power at higher degrees.

p0345 b0005 Achache *et al.* (1987) used the same basis functions to model satellite data, but reduced the size of the linear system by recognizing that they fall to negligibly small values quickly with lateral distance from the point at which the solution is being calculated. They thus included only those related to data points close to the point of interest, reducing the dimensions of the matrix to be inverted from the number of data to the number of 'nearby' data points. Their recommendation is that points within a horizontal distance $3h$, where h is satellite altitude, be included. In addition, they used principal component analysis to stabilize the inversion of the resulting (smaller) matrix by including only those eigenvectors associated with the largest eigenvalues. The decision as to how many eigenvectors to include is subjective, but the eigenvalue spectrum shows a rapid fall-off for satellite data acquired above 200-km altitude, making the choice relatively clear-cut. Previously, b0825 Langel *et al.* (1984) used principal component analysis to stabilize the calculation of ES solutions.

p0350 Based on methods originally developed for modeling seamount magnetism (b1205 Parker *et al.*, 1987), then adapted to account for crustal magnetization when modeling the main field (b0685 Jackson, 1990, b0690 1994), b1790 Whaler and Langel (1996) used a depleted basis minimum norm method to model crustal magnetization from satellite anomaly field data sets. Data are related to magnetization varying continuously in a crust of assumed constant thickness through [1], and hence the solution is expressed as a linear combination of the Green's functions

$$-\hat{\mathbf{l}}_j^{(\eta)} \cdot \nabla_{\mathbf{r}_j} \left\{ \frac{\mu_0}{4\pi} \nabla_{\mathbf{s}} \frac{1}{|\mathbf{r}_j - \mathbf{s}|} \right\} \qquad [11]$$

p0355 The resulting Gram matrix elements have closed-form expressions involving elliptic integrals, but these can be approximated very accurately by expressions involving only elementary functions since the thickness of the magnetized layer is small in comparison to the Earth's radius. A similar simplification applies if depth-independent magnetization is assumed; this is more appropriate for satellite data modeling, since the thickness of the magnetized layer is very much smaller than satellite altitude, so it is indistinguishable from a thin sheet. The norm minimized was

$$||\mathbf{M}|| = \sqrt{\int_v \mathbf{M} \cdot \mathbf{M} \, dv} \qquad [12]$$

that is, the root-mean-square (rms) magnetization amplitude of the crust. The method makes no assumption about the magnetization direction, so allows both remanent and induced magnetization. b1790 Whaler and Langel (1996) chose the same data set and distribution of depleted basis points b1785 Whaler (1994) used to downward continue the magnetic field to produce a magnetization model for Africa. For ease of comparison with ES dipole models assuming purely induced magnetization, they displayed the model as components in the direction of the main field (consistent with induced magnetization, or remanent magnetization acquired in today's main field), perpendicular to the main field in the meridian plane, and perpendicular to the meridian plane. b1790 Whaler and Langel (1996) note that by damping least-squares ES inversion, the solution minimizes the same norm as they employed, that is, minimum rms magnetization. The largest component of magnetization was in the direction of the current main field (or antiparallel to it), but the component of magnetization perpendicular to the main field in the meridian plane was also significant in many areas. The smallest component (perpendicular to the meridian plane) requires rotation and translation of the magnetization vector from that which would be recorded by rocks acquiring a contemporary remanent magnetization.

p0360 A similar difficulty of loss of resolution of the solution and subjectivity of the choice of depleted basis points can be overcome in the same fashion as for HS: by employing the iterative conjugate gradient technique to solve the full data-by-data system of equations, taking advantage of the sparseness of the matrix relating data to model parameters. Again, AU24 comparisons between b1790 Whaler and Langel's (1996) depleted basis magnetization model for Africa and surrounds and the equivalent part of the global conjugate gradient model of b1795 Whaler *et al.* (1996) are favorable. b1800 Whaler and Purucker (2005) have applied AU25 this technique to Martian orbiting satellite data, and compared the model to b0830 Langlais *et al.*'s (2004) ES dipole model. Mars no longer has an active dynamo, so the magnetization direction is unknown. b0830 Langlais *et al.* (2004) developed an iterative technique that allowed them to solve for both the amplitude and

direction of ES dipoles. Convergence was difficult to achieve, particularly as the dipole spacing was reduced, so their final model had a coarser spacing than the separation between the data points. Nonetheless, there was good agreement between their model and Purucker and Whaler's (2005) model, which was also based on a slightly different data set.

p0365 AU26 Spherical cap harmonic analysis (SCHA) (Haines, 1985), and the related translated origin spherical cap harmonic analysis (TOSCA) (de Santis, 1991), have been developed to model the field over small patches of the globe. As for global SHA, the potential is expressed as a finite sum of spherical harmonics, but including harmonics of noninteger degree. Assuming the cap is centered on $\theta = 0$ and subtends an angle θ_0 at the center of the Earth, the possible values of degree, n_k, which is a function of order, m, are those for which θ_0 is a zero of either $P^m_{n_k}(\theta)$ or $\partial P^m_{n_k}(\theta)/(\partial\theta)$. SCHA maps harmonics on the sphere to the spherical cap, so their effective wavelength is reduced accordingly. Thus, smaller-scale features can be represented over the cap with fewer coefficients than are required for global SHA. TOSCA moves the origin from the center of the Earth toward the surface along a line joining the Earth's center to the center of the cap. This adjusts the wavelength represented by a given harmonics to be smaller at the center of the cap than at the edge, an advantage if the data distribution is concentrated toward the center of the region. Korte and Holme (2003) present a method for regularizing SCHA, pointing out that, unlike SHA, the basis functions are not orthogonal. This means that it is not possible simultaneously to represent the potential for the vertical and horizontal field components exactly. Analytic continuation is prone to errors that increase with the upward or downward continuation distance, although Thebault *et al.* (2004) have re-posed SCHA as a boundary value problem within a cone extending above the reference surface, thereby allowing satellite data to be downward continued to the Earth's surface.

s0125 5.06.5.4 Transformations

p0370 The transformations of the next few subsections are applicable to 2-D data sets expressible in a rectangular geometry, such as those recorded in regional aeromagnetic surveys. They are most easily considered and performed in the wave number domain. The development here follows that of Gunn (1975) closely, but beware of typographical errors in his manuscript. We begin with the expression for the magnetic scalar potential V resulting from a distribution of magnetization $\mathbf{M}$ within an infinite half-space. Assuming a uniform direction of magnetization, the potential is (in Cartesian coordinates, with z positive downwards)

$$V(x,y,z) = \frac{\partial}{\partial k_0}\int_0^\infty \int_{-\infty}^{\infty}\int_{-\infty}^{\infty} \frac{M(\alpha,\beta,\gamma)}{d}\,\mathrm{d}\alpha\,\mathrm{d}\beta\,\mathrm{d}\gamma \quad [13]$$

where $\partial/\partial k_0$ is the derivative in the direction of $\mathbf{M}$, and d is the source–observation distance:

$$d^2 = (x-\alpha)^2 + (y-\beta)^2 + (z-\gamma)^2 \quad [14]$$

The α, β integral is a convolution, that is,

$$\int_{-\infty}^{\infty}\int_{-\infty}^{\infty} \frac{M(\alpha,\beta,\gamma)}{d}\,\mathrm{d}\alpha\,\mathrm{d}\beta \equiv M(x,y,\gamma)^* R(x,y,z-\gamma) \quad [15]$$

where '*' denotes convolution and

$$R(x,y,z-\gamma) = \frac{1}{\sqrt{x^2+y^2+(z-\gamma)^2}} \quad [16]$$

Hence, the Fourier transform of V is

$$\tilde{V}(u,v,z) = \frac{\partial}{\partial k_0}\int_0^\infty \tilde{M}(u,v,\gamma)\cdot\tilde{R}(u,v,z-\gamma)\mathrm{d}\gamma \quad [17]$$

where

$$\tilde{M}(u,v,\gamma) = \int_{-\infty}^{\infty}\int_{-\infty}^{\infty} M(x,y,\gamma)\mathrm{e}^{-\mathrm{i}(ux+vy)}\mathrm{d}x\,\mathrm{d}y \quad [18]$$

is the Fourier transform of $\mathbf{M}$, using the tilde symbol to denote Fourier-transformed quantities. The Fourier transform of R is

$$\int_{-\infty}^{\infty}\int_{-\infty}^{\infty} \frac{1}{\sqrt{x^2+y^2+(z-\gamma)^2}}\mathrm{e}^{-\mathrm{i}(ux+vy)}\mathrm{d}x\,\mathrm{d}y = 2\pi\frac{\mathrm{e}^{(z-\gamma)\sqrt{u^2+v^2}}}{\sqrt{u^2+v^2}} \quad [19]$$

and so

$$\tilde{V}(u,v,z) = 2\pi\frac{\partial}{\partial k_0}\int_0^\infty \tilde{M}(u,v,\gamma)\frac{\mathrm{e}^{(z-\gamma)\sqrt{u^2+v^2}}}{\sqrt{u^2+v^2}}\mathrm{d}\gamma \quad [20]$$

Let (l, m, n) be the direction cosines of $\mathbf{M}$. Then

$$\frac{\partial}{\partial k_0} = l\frac{\partial}{\partial x} + m\frac{\partial}{\partial y} + n\frac{\partial}{\partial z} \quad [21]$$

But $\partial f/\partial x = \mathrm{i}u\tilde{f}$ for any Fourier transform pair f, $\tilde{f}$(and similarly for differentiation with respect to y). Hence

$$\tilde{V}(u,\ v,\ z) = 2\pi \frac{ilu + imv + n\sqrt{u^2+v^2}}{\sqrt{u^2+v^2}} \times \int_0^\infty \tilde{M}(u,v,\gamma)\mathrm{e}^{(z-\gamma)\sqrt{u^2+v^2}}\,\mathrm{d}\gamma \quad [22]$$

We now need to relate the (Fourier transformed) potential V to the (Fourier transformed) component of the magnetic field being measured, usually that in the direction of **F**, which we take to have direction cosines $(l',\ m',\ n')$:

$$\Delta T(u,\ v,\ z) = 2\pi \frac{\left[ilu + imv + n\sqrt{u^2+v^2}\right]\left[il'u + im'v + n'\sqrt{u^2+v^2}\right]}{\sqrt{u^2+v^2}} \times \int_0^\infty M(u,v,\gamma)\mathrm{e}^{(z-\gamma)\sqrt{u^2+v^2}}\mathrm{d}\gamma \quad [23]$$

It is easily shown that $l = \cos I_\mathrm{F} \cos D_\mathrm{F}$, $m = \cos I_\mathrm{F} \sin D_\mathrm{F}$, and $n = \sin I_\mathrm{F}$, where I_F and D_F denote the inclination and declination of the main field, respectively, and similarly for $(l',\ m',\ n')$.

s0130 p0375

5.06.5.4.1 Analytic continuation

From [23] it follows straightforwardly that analytic (upward or downward) continuation involves convolving with a filter whose frequency response is e^{Hk}, that is, multiplying by e^{Hk} in the wave number domain, where $k^2 = u^2 + v^2$ is the square of the wave number, and H is the continuation height or depth (also measured positive downwards). e^{Hk} is sometimes referred to as the analytic continuation operator. Thus, downward continuation is an amplifying and roughening operation (conversely for upward continuation). This is analogous to the spherical case where the amplification factor is $(a/r)^{n+2}$, where n is spherical harmonic degree, a is the reference radius of the spherical harmonic expansion, and r the analytic continuation radius. Examples of the uses of analytic continuation are to suppress or enhance short-wavelength features, reduce data collected at a variety of altitudes (e.g., different flying heights for airborne surveys) to constant height, either above terrain or relative to mean sea level, compare ground and airborne observations, and estimate depth to sources (see Section 5.06.5.5).

s0135 p0380

5.06.5.4.2 Reduction to the pole

Reduction to the pole (RTP) is achieved by convolving with a filter whose frequency response is

$$\frac{\sqrt{u^2+v^2}}{ilu + imv + n\sqrt{u^2+v^2}} \cdot \frac{\sqrt{u^2+v^2}}{il'u + im'v + n'\sqrt{u^2+v^2}} \quad [24]$$

(the factor $\sqrt{u^2+v^2}$ in each term preserves dimensions), that is, [24] is the RTP operator (or filter). It removes the factors in [23] associated with the direction of the main field and the direction of remanent magnetization. Its effect is to reduce the anomalies to those that would be observed at the magnetic North pole with a vertical remanent magnetization direction. If the remanent magnetization direction is unknown, or magnetization can be assumed to be purely induced, the direction cosines of magnetization are replaced by those of the main field. RTP becomes unstable as the magnetic equator is approached since the numerator of [24] approaches zero (recall $n = \sin I_\mathrm{F}$). At low magnetic latitudes, it is possible to perform reduction to the equator instead, but the form of the resulting anomalies is not as simple as for RTP. Silva (1986)[b1570] has treated RTP as an inverse problem, using methods designed for stabilizing inversion to stabilize RTP. Besides aiding interpretation through simplifying the form of the anomalies and centering them over their causative structures, RTP eases the comparison of oceanic magnetic anomalies at different latitudes.

s0140 p0385

5.06.5.4.3 Pseudogravity

The pseudogravity transformation follows from Poisson's relation between the magnetic potential and the gravitational field. Consider a body with uniform magnetization (both strength and direction) and density occupying a volume Ω. Then the magnetic scalar potential is

$$V(P) = -\mathbf{M} \cdot \nabla_P \int_\Omega \frac{1}{d}\mathrm{d}\Omega \quad [25]$$

where P is the observation point, and d is distance from P, and the gravitational potential is

$$U(P) = G\rho \int_\Omega \frac{1}{d}\mathrm{d}\Omega \quad [26]$$

where G is the gravitational constant. Combining the two,

$$V(P) = -\frac{1}{G\rho}\mathbf{M} \cdot \nabla_P U = -\frac{1}{G\rho} M g_\mathrm{M} \quad [27]$$

where g_M is the component of gravity in the direction of **M**; [27] is Poisson's relation. In fact, it is not necessary for the potential and magnetization to be constant. We can consider a body to be composed of arbitrarily small volumes in which density and

magnetization can be regarded as constant. Since potentials add, [27] applies to a body in which density and magnetization vary in proportion. However, pseudogravity is defined as the gravity anomaly that would be observed if the magnetization distribution were replaced by an identical density distribution, that is, M/ρ is a constant. In the wave-number domain, this gives

$$\tilde{g}_{\mathrm{M}} = C\tilde{V} \qquad [28]$$

where $C = -(G\rho/M)$ is a constant. Converting from the magnetic potential to total field anomaly,

$$\tilde{g}_{\mathrm{M}} = C\frac{1}{(il'u + im'v + n'\sqrt{u^2+v^2})}\Delta\tilde{T} \qquad [29]$$

Finally, converting from the component of gravity in the direction of **M** to the vertical component gives the Fourier-transformed pseudogravity, $\tilde{g}_{\mathrm{ps}}$:

$$\tilde{g}_{\mathrm{ps}} = C\frac{\sqrt{u^2+v^2}}{(ilu + imv + n\sqrt{u^2+v^2})(il'u + im'v + n'\sqrt{u^2+v^2})}\Delta\tilde{T} \qquad [30]$$

Thus, the pseudogravity operator is

$$\frac{\sqrt{u^2+v^2}}{(ilu + imv + n\sqrt{u^2+v^2})(il'u + im'v + n'\sqrt{u^2+v^2})} \qquad [31]$$

Note that, unlike the expression for the RTP operator, there is only one factor $\sqrt{u^2+v^2}$ in the numerator of [31] because Poisson's relation [27] relates the magnetic scalar *potential* to the component of the gravitational *field* in the direction of magnetization. This means that the pseudogravity operator alters the frequency content of the signal, preferentially amplifying the longer-wavelength components (in contrast to the spatial derivatives discussed in Section 5.06.5.4.4, which preferentially amplify the shorter-wavelength components). Like the RTP operator, it can run into problems at low magnetic field or magnetization inclinations. The constant C in [30] means we can predict the pattern (but not the amplitude) of the gravity anomalies that would be obtained over the same structure. The pseudogravity transformation aids the comparison of magnetic and gravity anomalies, allows gravity methods to be used to interpret magnetic anomalies, and can be used in conjunction with gravity data to determine the direction of magnetization and the ratio of magnetization to density (Cordell and Taylor, 1971). Note that Poisson's relationship provides an example of the ambiguity in magnetization modeling – there is no total field anomaly over a uniformly magnetized sheet (regardless of the direction of magnetization) since its gravity anomaly is constant. The result extends to a spherical geometry, where more complicated magnetization distributions can be shown to produce no external magnetic field (Runcorn, 1975). These magnetic annihilators are discussed more fully in Section 5.06.5.6.

5.06.5.4.4 Spatial derivatives

Derivatives are useful for enhancing smaller-scale features of a data set, and anomalies caused by shallow bodies, and directional derivatives for enhancing or suppressing features in a given direction. The second vertical derivative is valuable because it relates to second horizontal derivatives through Laplace's equation, which is satisfied by the total field anomaly as well as the scalar potential if the main field direction is constant. This involves multiplying $\Delta\tilde{T}$ by k^2 and is thus a significantly roughening operation. It is used to suppress regional gradients, and to aid in the determination of source depth and the attitude of interfaces. As noted above, differentiation with respect to x or y multiplies $\Delta\tilde{T}$ by iu or iv, respectively. The horizontal derivative, that is, the derivative in the direction of maximum change, therefore has a Fourier transform $k\Delta\tilde{T}$. This follows because

$$\nabla\Delta T = \frac{\partial\Delta T}{\partial x}\mathbf{i} + \frac{\partial\Delta T}{\partial y}\mathbf{j} \qquad [32]$$

where $\mathbf{i}$, $\mathbf{j}$ are unit vectors in the x-, y-directions, respectively. Thus in the wave-number domain

$$\nabla\Delta\tilde{T} = iu\Delta\tilde{T}\mathbf{i} + iv\Delta\tilde{T}\mathbf{j} \qquad [33]$$

and hence

$$\left|\nabla\Delta\tilde{T}\right| = \sqrt{\nabla\Delta\tilde{T}^{*}\nabla\Delta\tilde{T}} = k\Delta\tilde{T} \qquad [34]$$

where here * denotes complex conjugate. First derivatives are also required in some methods of estimating depth to sources (see, e.g., Section 5.06.4.7). Directional derivatives, for example, in the direction defined by an angle φ_0 with the x-axis, are obtained by taking the magnitude of $\cos\varphi_0$ times the x-derivative, and $\sin\varphi_0$ times the y-derivative. Directions are preserved on Fourier transformation: since the wave vector $\mathbf{k}$ has components u and v in

the x- and y-directions respectively, its magnitude is $\sqrt{u^2 + v^2}$ and its phase is

$$\tan \varphi_0 = \frac{v}{u} = \frac{y}{x} \qquad [35]$$

the latter by definitions of φ_0. Thus, the directional derivative enhances features making an angle φ_0 with the x-axis; to suppress them, but still improve the definition of smaller-scale features, one could take the directional derivative in the orthogonal direction.

s0150 ***5.06.5.4.5 Pie-crust filter***

p0395 An alternative method of eliminating anomalies in a particular direction is to use the pie-crust filter or operator, given by

$$W(\varphi) = \begin{cases} 0 & (\varphi_0 - \Delta\varphi < \varphi < \varphi_0 + \Delta\varphi) \\ 0 & (\varphi_0 - \Delta\varphi < \varphi + \pi < \varphi_0 + \Delta\varphi) \\ 1 & \text{otherwise} \end{cases} \qquad [36]$$

This removes anomalies within an angle $\Delta\varphi$ either side of φ_0, and preserves those at all other angles, without altering the frequency content. Anomalies within this wedge can be preserved by swapping the values 0 and 1 in [36]. A more sophisticated filter (with a taper between 0 and 1) would reduce ringing when the filtered anomalies are transformed back to the spatial domain.

s0155 ***5.06.5.4.6 Analytic signal***

p0400 Another useful interpretational tool is the analytic signal, defined as

$$\mathbf{A}(x,y) = \frac{\partial \Delta T}{\partial x}\mathbf{i} + \frac{\partial \mathrm{T}}{\partial \mathrm{y}}\mathbf{j} + i\frac{\partial \mathrm{T}}{\partial \mathrm{z}}\mathbf{k} \qquad [37]$$

where **i**, **j**, and **k** are unit vectors in the x-, y-, and z-directions respectively. The real and imaginary parts of its Fourier transform are the horizontal and vertical derivatives of ΔT, respectively. They form a Hilbert transform pair, as required for **A** to be an analytical signal, a property most easily demonstrated in the wave-number domain (Roest *et al.*, 1992). The amplitude of the analytic signal

$$|\mathbf{A}(x,y)|^2 = \sqrt{\left(\frac{\partial \Delta T}{\partial x}\right)^2 + \left(\frac{\partial \Delta T}{\partial y}\right)^2 + \left(\frac{\partial \Delta T}{\partial z}\right)^2} \qquad [38]$$

is most often used for interpretation. It has maxima at magnetization contrasts, independent of the direction of the ambient magnetic field for 2-D sources and only weakly dependent on these directions for 3-D sources, offering a method for locating the edges of magnetized bodies. If the edges are assumed vertical, it can be used to determine depth to sources. Over a 2-D vertical contrast in magnetization at depth d, the amplitude of the analytic signal is proportional to $1/(x^2 + d^2)$ where x is the horizontal distance from the contact (Nabighian, 1972). Thus the half-width of the curve gives d, the depth to the contrast. Automatic methods for finding the positions of maxima of quantities such as the analytic signal are given by Blakeley and Simpson (1986). Other boundary edge finding methods include the terracing operator of Cordell and McCafferty (1989) and the 'amplitude of horizontal gradient method' of Cordell and Grauch (1985).

5.06.5.4.7 Euler deconvolution s0160

Euler's homogeneity equation can be written (e.g., Reid *et al.*, 1990) p0405

$$(x - x_0)\partial\Delta T/\partial x + (y - y_0)\partial\Delta T/\partial y + (z - z_0)\partial\Delta T/\partial z = -s_i \Delta T \qquad [39]$$

Here, (x, y, z) is the position at which the total field anomaly is ΔT, arising from a source at position (x_0, y_0, z_0). S_i is the 'structural index' (SI), a measure of the rate of fall-off of the field with distance, which therefore reflects the source geometry (Thompson, 1982). An SI of 3 corresponds to a point source (dipole), 2 is appropriate for extended line sources, such as pipes and cylinders, a value of 1 for a step, thin dike or sill edge, and values of 0.5 and 0 have been chosen for faults and other contacts. If N is set to zero, the right-hand side of [39] should be replaced by a constant, which depends on the amplitude of the contrast in magnetization, and the strike and dip of the contact (Reid *et al.*, 1990).

p0410 Euler deconvolution (which is not strictly a deconvolution) has proved itself particularly useful in a regional context, when grids or profiles of data can be inverted systematically for source parameters and the background field (or the constant on the right-hand side of [39] when $N = 0$). As [39] shows, the method requires derivatives of ΔT, which are usually calculated in the wave-number domain. These are treated as data (along with the SI) in an inversion for the source positions and background field (or right-hand side constant). Obtaining useful solutions depends on careful choice of the window size (i.e., how many adjacent points are included in a single least-squares-type inversion). Each window produces a set of source parameters, and only those with standard deviations below a specified threshold

are retained. Even these often plot as quasi-linear features ('strings of pearls'), that is, the solutions tend to be defocused. This may be partly because a region often includes sources represented by more than one SI, and attempts have been made to develop a multiple source approach. Other approaches include methods of determining automatically, or also solving for, SI, for example, wavelet-based methods for estimating degree of homogeneity (Sailhac *et al.*, 2000). The usual methods of damping and generalized inverses are useful in improving the performance of the method and interpretation of the results (e.g., Neil *et al.*, 1991; Mushayandebvu *et al.*, 2004), but damping tends to bias depth estimates.

Several authors have pointed out that Euler deconvolution can be applied to any homogeneous field or function. This includes the horizontal gradient or analytic signal of a field that is itself homogeneous, for example, the magnetic field, or its Hilbert transform; the appropriate SI for the horizontal gradient or analytic signal is then one larger than that of the original field source. The advantage of deconvolving the analytic signal rather than the magnetic field itself is that its calculation effectively removes the background field.

5.06.5.5 Forward and inverse methods

Transformations assist in the characterization of certain features of the magnetic source, thereby facilitating interpretation. Forward and inverse methods take this characterization a step further, determining attributes of the magnetic source. Forward methods begin with one or more magnetic bodies whose salient features are selected *a priori*, on the basis of geologic or geophysical knowledge. Magnetic fields are then predicted for these bodies at the survey location, and model parameters are adjusted on the basis of the closeness of the fit to the observation. This process continues until a sufficiently close fit to the observations is achieved. Inverse methods, in contrast, allow for the direct determination of one or more attributes of the magnetic source, usually through least-squares or Fourier-transform techniques.

5.06.5.5.1 Forward models

Procedures for calculating magnetic forward models involve simplification of complex bodies into simpler ones, either as collections of rectangular prisms (Bhattacharyya, 1964), magnetic dipoles (Dyment and Arkani-Hamed, 1998), polygonal laminae (Talwani, 1965; Plouff, 1976), or polyhedrons (Bott, 1963). The calculation can be made either in the space or wave-number domains. Parker (1973) gives a wave-number domain-based algorithm for the rapid calculation of the crustal magnetic field over sources defined by a magnetization contrast over a topographic surface.

5.06.5.5.2 Inverse approaches

Quantitative interpretations sought using an inverse approach aim to estimate the causative body's depth, dimension, and magnetization contrast. In many applications, depth to the magnetic source is the most important of these properties. Depth to source determinations are of two types: (1) based on the shape of individual anomalies (beginning with Peters, 1949), and (2) based on the statistical properties of ensembles of anomalies (beginning with Spector and Grant, 1970), and implemented in the spectral domain.

The first analytic approximation to determining the depth to source was by Werner (1955), who solved the problem under the assumption that the source was a thin dike. Subsequent work has relaxed that limitation, and allowed for other source geometries (Ku and Sharp, 1983). The exploitation of Euler's homogeneity relation [39] led to a second class of analytic approximations (Reid *et al.*, 1990). This approximation allows for a variety of sources to be treated successfully, as outlined in section 5.06.4.7.

Wave-number-domain approaches to individual anomalies include the methods of Naudy (1971), applicable to a vertical dike or thin plate, and CompuDepth (O'Brien, 1972).

5.06.5.5.2.(i) Fourier domain approaches to groups of anomalies

Matched Filters (Syberg, 1972; Phillips, 1997) use the Fourier-domain properties (Spector, 1968; Spector and Grant, 1970) of the magnetic field to estimate the depths of the principal sources. These depths are then used to design wavelength filters, which are in turn used to decompose observed magnetic anomalies into estimates of the anomalies caused by sources at those principal depths. The original Spector and Grant (1970) method estimated the depth from the slope of the radially averaged power spectrum.

5.06.5.6 Resolving Interpretational Ambiguity

Some of the ways for resolving or better understanding interpretational ambiguity include annihilators

(Runcorn, 1975; Maus and Haak, 2003), ideal body analysis (Parker, 2003), Monte Carlo simulations (Sambridge and Mosegaard, 2002), and, of course, through the use of prior information.

p0455 It has long been known that an infinite sheet with constant magnetization produces no magnetic field outside of the sheet, although second-order effects usually ensure that some magnetic fields escape. Only magnetization contrasts produce magnetic fields. Runcorn (1975) demonstrated, in the case of the moon, that a spherical shell of constant susceptibility linearly magnetized by an arbitrary internal field also produces no field outside of the shell. More recently, Maus and Haak (2003) illustrated another class of magnetization solutions that produce no external fields. Their example, based on reasoning from spherical harmonics, is one defined by a magnetic susceptibility profile in a dipolar field that is symmetric about the magnetic equator. In the case of the Earth, South America and Africa are approximately bisected by the magnetic dipole equator, and their shape can be approximated fairly well by an annihilator. Thus, if these continents possess a large-scale magnetic contrast with the surrounding ocean, much of that contrast may be invisible. It is expected that further inquiry will reveal additional classes of annihilators.

p0460 The theory of ideal bodies (Parker, 1974, 1975) systematizes the process of placing bounds on the parameters of the source region, such as the depth of burial (Grant and West, 1965). The process for doing this involves the minimization of the infinity norm of the magnetic intensity $|\mathbf{M}|$ within the source region. Parker (2003) showed how such a process could be used to determine the distribution of magnetization that has the smallest possible intensity, without any assumptions about its direction.

p0465 The Metropolis algorithm and the Gibbs sampler (Mosegaard and Sambridge, 2002) are Monte Carlo techniques for the exploration of the space of feasible solutions. They also provide measures of resolution and uncertainty. Although not widely used in the field of crustal magnetism, the Metropolis algorithm has been used by Rygaard-Hjalsted *et al.* (2000) to conduct resolution studies on fluid flow in the Earth's outer core from geomagnetic field observations. Monte Carlo techniques can also be used to find globally optimal AU31 solutions, and Dittmer and Szymanski (1995) have applied simulated annealing to magnetic and resistivity data.

5.06.6 Spectral Overlap with Other Fields s0190

p0470 The transition from core-dominated to crust-dominated processes occurs as a relatively sharp break centered at spherical harmonic degree 14 (Alldredge *et al.*, 1963; Cain *et al.*, 1974; Langel and Estes, 1982) corresponding to wavelengths of $40\,000/14 = 2860$ km. This transition can be seen in a power spectrum of the static field (**Figure 8**). The crustal field is much stronger over the continents than over the oceans (Arkani-Hamed and Strangway, 1986; Hinze *et al.*, 1991) and so we expect that the spectral overlap with the core field will be different for continental than for oceanic crust. The crustal field is expected to have power at wavelengths longer than degree 14 because of the markedly different characteristics of continental and oceanic crust (Meissner, 1986) and because of long-wavelength oceanic magnetic anomalies (Dyment and Arkani-Hamed, 1999). These longest wavelengths are masked by the dominant core fields (Hahn and Bosum, 1986), and various forward (Cohen, 1989) and inverse (Purucker *et al.*, 1998, 2002) approaches have been developed in an attempt to include at least some notional idea of these fields. The longest-wavelength crustal magnetic fields remain inaccessible to direct observation, although Mayhew and Estes (1983) suggest that simultaneous modeling of core and crustal fields using ES dipole arrays located both within the core and crust might make possible the separation of the sources. The task they outlined is now computationally feasible (Purucker *et al.*, 1996), but there are reasons for suspecting that a full separation may not be possible. For example, it is possible to represent magnetic fields of long wavelength (say the dimension of a continent) by ES dipoles placed either at the surface, or at the core–mantle boundary. A separation based solely on the radial position of the dipoles is thus likely to be ill-posed, and depend on details of the parameterization, such as the tessellation used, its spacing, and the distance over which the observations are expected to influence the crustal dipoles. The debate over the existence of field-aligned current systems (Dessler, 1986) shows the difficulty of interpreting physically an equivalent current/dipole system deduced solely from observations of the magnetic field.

p0475 On the other hand, co-estimation of magnetic fields of internal and external origin through the 'comprehensive model' approach (Sabaka *et al.*,

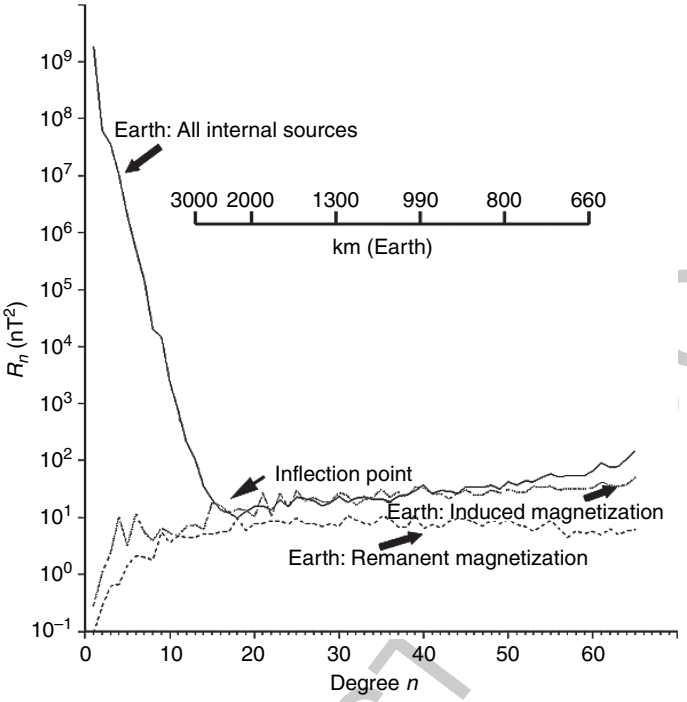

f0040 **Figure 8** Comparison of the Lowes-Mauersberger (R_n) spectra at the surface of the Earth for a variety of internal fields. The inflection point in the terrestrial power spectra represents the sharp transition from core processes at low n to lithospheric processes at higher n. R_n is the mean square amplitude of the magnetic field over a sphere produced by harmonics of degree n. The spectrum of all internal sources comes from Sabaka *et al.* (2004), the induced spectrum is derived from Fox Maule *et al.* (2005), and the remanent magnetization spectrum (of the oceans, and hence a minimum value) was derived from Dyment and Arkani-Hamed (1998).

2002, 2004; Olsen *et al.*, 2006a) has been successful because of the different decay characteristics of the internal and external fields (Langel *et al.*, 1996). This approach utilizes magnetic field measurements from satellites (ionosphere, crust, and core are internal) and the surface (crust and core are internal), and does not separate the internal fields of core and crustal origin, lumping them instead into a spherical harmonic series from spherical harmonic degrees 1–60. These 'comprehensive' models are now widely touted (Nabighian *et al.*, 2005) to replace the existing International Geomagnetic Reference Field Models in many applications.

p0480 Another, qualitative, approach to separation is to characterize visually the field, and magnetization solutions deduced from that field, in the hope that features at small scales will provide clues into what is happening at the largest scales. Because of the wider spectral content of recent satellite crustal field models, Purucker and Whaler (2004) were able to recognize two patterns in the vertical component map (**Figure 9**) of the crustal field of the North American region.

p0485 The first pattern, which they refer to as 'C', encompasses the North American land mass, the Caribbean and Gulf of Mexico, and northernmost South America. The peak-to-trough magnitude of anomalies in 'C' typically exceeds 50 nT, and the anomalies are either equidimensional or oriented in a direction subparallel to the nearest coastline or tectonic element. The second pattern, which they refer to as 'O', encompasses the Eastern Pacific, the Cocos plate, and the western Atlantic away from continental North America. The peak-to-trough magnitude of anomalies in 'O' is typically less than 30 nT, and the anomalies are commonly narrow and elongate in the direction of the nearest spreading or subduction zone. The 'C' pattern can also be discerned on global maps of the field, when account is taken of the higher altitude. The 'C' pattern is characteristic of much of the Asian landmass, a region centered on but more extensive than Australia, and two broad regions within the African landmass. The 'O' pattern is seen in the eastern Pacific, the North and South Atlantic, and the Indian oceans. The 'C' and 'O' patterns are also evident in a magnetization

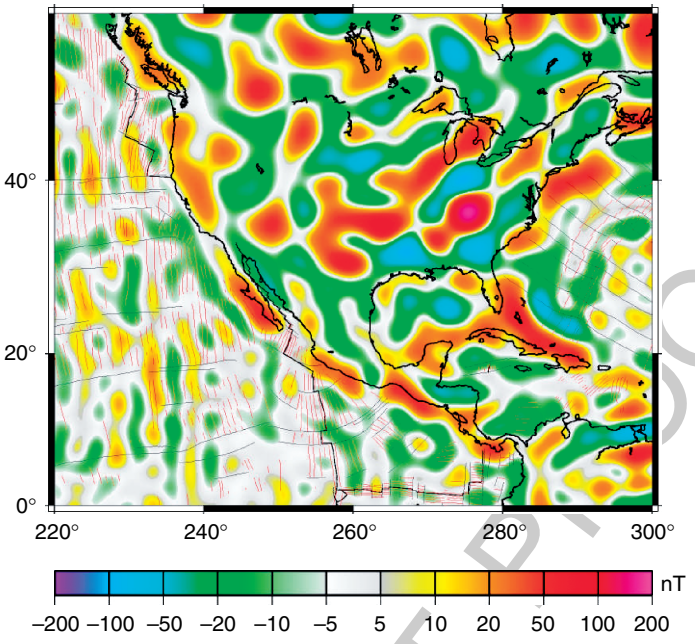

f0045 **Figure 9** MF-4 vertical field map of the crustal magnetic field (Maus *et al.*, 2006) over North America, evaluated at 50 km altitude.

model based on these observations (b1365 Purucker and Whaler, 2004). A map of $|\mathbf{M}|$ shows these patterns best (**Figure 10**). Regions with magnetizations greater than $0.1\,\mathrm{A\,m^{-1}}$ (red regions on **Figure 10** map) correspond to the 'C' pattern, and regions with magnetization less than $0.06\,\mathrm{A\,m^{-1}}$ (gray regions) correspond to the 'O' pattern.

p0490 Intermediate values of magnetization (between 0.06 and $0.1\,\mathrm{A\,m^{-1}}$, pink on above map) generally envelop regions displaying the 'C' pattern. In a general way, the 'C' and 'O' patterns correspond to regions of thick and thin magnetic crustal thickness, as defined by temperature and seismology in the 3SMAC model (b1095 Nataf and Ricard, 1996). There are conspicuous exceptions to this generalization. Most of the South American landmass south of the Equator is characterized by the 'O' pattern, yet crustal thicknesses are typical of continental crust. The other major exception is the Sahara desert, again characterized by the 'O' pattern but with typical continental crustal thicknesses. In both of these regions, seismic crustal thickness and heat flow are poorly known.

Electrical conductivity contrasts (b1495 Grammatica and Tarits, 2002) and motional induction by ocean p0495

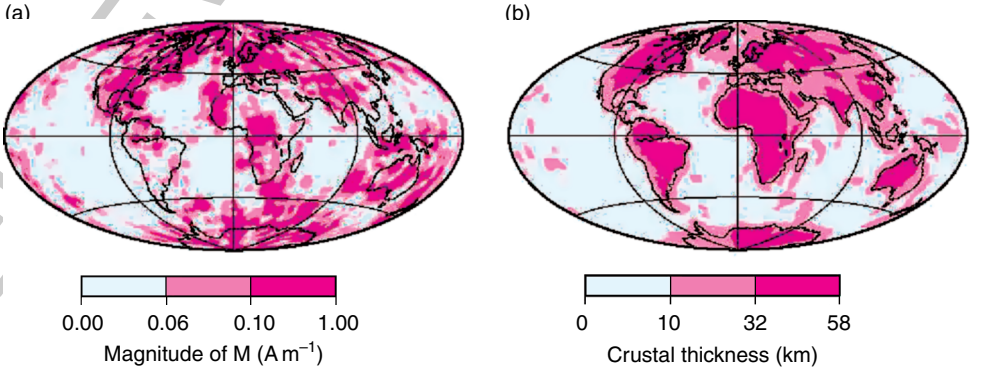

f0050 **Figure 10** Map showing the magnitude (a) of the magnetization inferred from a model based on MF-3 (Maus *et al.*, 2006), compared with a map of the magnetic crustal thickness (b) from Nataf and Ricard (1996).

currents (Vivier *et al.*, 2004) can also produce quasi-static magnetic fields that overlap with the crustal field. Specific time-variable features of these fields makes separation possible, but their low amplitude makes separation difficult in practice, and no separation has yet been achieved.

5.06.7 Separation of Induced and Remanent Magnetization

p0500 Separation of induced and remanent magnetization is a major outstanding issue. Induced magnetizations in the crust represent one of the largest time-variable geomagnetic fields of internal, non-core origin, and the separation of induced from remanent magnetization remains an area of active research. McLeod (1996) predicted that crustal-source secular variation should dominate core-source secular variation for spherical harmonic degrees in excess of 22. The separation of induced from remanent magnetization can be done without ambiguity only if the source material is available for rock magnetic tests (cf. 00093), and if the time scale is specified. Although magnetizations are often considered either remanent or induced, the distribution of magnetic coercivities in rocks is a continuous function, and viscous remanent magnetizations exist at all time scales.

p0505 Both the spatial variability of the static field as a function of inducing field, and an approach using time-variable geomagnetic fields as a probe, have been used to estimate induced magnetizations. Maus and Haak (2002) investigated the long-wavelength power of the crustal field as a function of magnetic dip latitude. Two of the crustal magnetic field models (Sabaka *et al.*, 2002; Cain *et al.*, 1989) they examined showed the strong trend with latitude expected for induced magnetization, while the third model (Arkani-Hamed *et al.*, 1994) they examined was consistent with a purely remanent magnetization. It may be relevant that the models that were consistent with induced magnetization were models of both internal (core and crust) and external fields, while the model that was consistent with remanence was a crustal-only model that employed along-track filtering to remove non-crustal(?) long-wavelength trends. Maus and Haak (2002) also showed that, even in the case of a purely remanent magnetization, ΔT is expected to increase by a factor of two between the equator and the pole, while for a purely induced magnetization, ΔT is expected to increase by a factor of 32/3 (almost 11) between the equator and the pole. This is due to the preferential sampling of the weaker tangential part of the crustal field at the equator and the stronger radial part at the poles.

p0510 Approaches using time-variable geomagnetic fields can be either direct, using the change of the main geomagnetic field, or indirect, using an EM induction response (Goldstein and Ward, 1996; Yanovsky, 1938; Clark *et al.*, 1998) to time-variable fields like Sq or micropulsations. Lesur and Gubbins (2000) take a direct approach, with a regional study of 20 long-running European observatories. They calculate the difference between the observatory annual mean and the core field model of Bloxham and Jackson (1992). The variability with time of that difference, or observatory bias, was then examined to see if it was consistent with induced or remanent magnetization. They found that for nine observatories a time-dependent induced field fit the data better than a steady remanent field at the 99% confidence level. The other observatories yielded ambiguous results. Some external field signatures remain in observatory annual mean data, and only local distributions of induced and remanent magnetization were considered in the analysis. A global approach to observatory biases by Mandea and Langlais (2002), for observatories operating while the Magsat (1980) and Orsted (2000) missions were in operation, while not attempting to isolate the remanent and induced components, illustrates some of the other difficulties that the direct approach entails. In addition to contamination by external fields, changes in observatory location or measurement practice add to the uncertainty. One can estimate the magnitude of the change in the observatory bias between the Magsat and Orsted epochs, assuming that it is caused solely by changes in the induced magnetization. Values can be large as 77 nT, with 14 of the 62 observatories having predicted changes in excess of 5 nT. Such a large signal over only 20 years should be measurable, assuming that it can be isolated. Although Mandea and Langlais (2002) determine the biases *a posteriori* the model generation, they could also be solved for in a model, as for example in the Comprehensive model of Sabaka *et al.* (2002).

p0515 The separation of induced and remanent magnetization can also be attempted from the spatial distribution of ΔT over isolated magnetic bodies (Zietz and Andreasen, 1967). Zietz and Andreasen (1967) used the position and relative intensity of the maximum and minimum anomaly to infer the declination and inclination of the magnetization vector in

the causative body. Schnetzler[b1530] and Taylor (1984) evaluated this technique globally, and found that the method was more sensitive at higher magnetic latitudes, and that due to zero-level uncertainties, inclination was very difficult to estimate.

Acknowledgments

Purucker is supported under NASA Contract NNG06HX08C. All graphs and maps have been plotted using the Generic Mapping Tools (GMT) software (Wessel[b1780] and Smith, 1998).

References

b0005 Achache JA, Abtout A, and Le Mouël JL (1987) The downward continuation of MAGSAT crustal anomaly field over Southeast Asia. *Journal of Geophysical Research* 92: 11584–11596.

b0010 Adam JC and Swarztrauber PN (1997) Spherepack 2.0: A model development facility. *NCAR Technical Note NCAR/TN-436-STR*.

b0015 Alldredge LR (1981) Rectangular harmonic analysis applied to the geomagnetic field. *Journal of Geophysical Research* 86: 3021–3026.

b0020 Alldredge LR (1982) Geomagnetic local and regional harmonic analysis. *Journal of Geophysical Research* 87: 1921–1926.

b0025 Alldredge LR, Vanvoorhis GD, and Davis TM (1963) A magnetic profile around the world. *Journal of Geophysical Research* 68: 3679–3692.

b0030 Andreasen G E and Zietz I (1969) Magnetic fields for a 4×6 prismatic model. *US Geological Survey Professional Paper 666.* Washington, DC: US Geological Survey.

b0035 Arctic Gravity Project (2002) $5' \times 5'$; grids compiled by the International Association of Geodesy from airborne, survey, and submarine surveys. [http://earth-info.nga.mil/GandG/wgs84/agp/readme.html]. (accessed Nov 2006).

b0040 Arkani-Hamed J, Langel R, and Purucker M (1994) Scalar magnetic anomaly maps of Earth derived from POGO and Magsat data. *Journal of Geophysical Research* 99: 24075–24090.

b0045 Arkani-Hamed J and Strangway D (1986) Band-limited global scalar magnetic anomaly map of the Earth derived from Magsat data. *Journal of Geophysical Research* 91: 8193–8203.

b0050 Aspler LB, Pilkington M, and Miles WF (2003) Interpretations of Precambrian basement based on recent aeromagnetic data, Mackenzie Valley, Northwest Territories. *Geological Survey of Canada Current Research* 2003-C2: 11.

b0055 Aydin I, Karat HI, and Kocak A (2005) Curie-point depth map of Turkey. *Geophysical Journal International* 162: 633–640.

b0060 Bankey V, Cuevas A, Daniels D, *et al.* (2002) Digital data grids for the magnetic anomaly map of North America, *USGS Open File Report 02-414*. http://pubs.usgs.gov/of/2002/ofr-02-414 (http://crustal.usgs.gov/geophysics). (accessed Nov 2006).

b0065 Baranov V (1957) A new method for interpretation of aeromagnetic maps; pseudo-gravimetric anomalies. *Geophysics* 22: 359–383.

b0070 Baranov V and Naudy H (1964) Numerical calculation of the formula of reduction to the magnetic pole. *Geophysics* 29: 67–79.

b0075 Barbosa VCF, Silva JBC, and Medeiros WE (1999) Stability analysis and improvement of structural index estimation in Euler deconvolution. *Geophysics* 64: 48–60.

b0080 Barritt SA, Fairhead JD, and Misener DJ (1993) The African Magnetic Mapping Project. *ITC Journal* 122–131. AU32

b0085 Bean RJ (1966) A rapid graphing solution for the aeromagnetic anomaly of a two-dimensional tabular body. *Geophysics* 31: 963–970.

b0090 Bhattacharyya BK (1964) Magnetic anomalies due to prism-shaped bodies with arbitrary polarization. *Geophysics* 29: 517–531.

b0095 Bhattacharyya BK (1965) Two-dimensional harmonic analysis as a tool for magnetic interpretation. *Geophysics* 30: 829–857.

b0100 Bhattacharyya BK (1966) Continuous spectrum of the total-magnetic-field anomaly due to a rectangular prismatic body. *Geophysics* 31: 97–121.

b0105 Bhattacharyya BK (1969) Bicubic spline interpolation as a method for treatment of potential field data. *Geophysics* 34: 402–423.

b0110 Bhattacharyya BK (1980) A generalized multibody model for inversion of magnetic anomalies. *Geophysics* 45: 255–270.

b0115 Bhattacharyya BK and Chan KC (1977a) Reduction of magnetic and gravity data on an arbitrary surface acquired in a region of high topographic relief. *Geophysics* 42: 1411–1430.

b0120 Bhattacharyya BK and Chan KC (1977b) Computation of gravity and magnetic anomalies due to inhomogeneous distribution of magnetization and density in a localized region. *Geophysics* 42: 602–609.

b0125 Blakely RJ (1981) A program for rapidly computing the magnetic anomaly over digital topography. *US Geological Survey Open File Report 81–298.*

b0130 Blakely RJ (1988) Curie-temperature isotherm analysis and tectonic implications of aeromagnetic data from Nevada. *Journal of Geophysical Research* 93: 11,817–11,832.

b0135 Blakely RJ (1995) *Potential Theory in Gravity and Magnetic Application*. New York: Cambridge University Press.

b0140 Blakely RJ, Brocher TM, and Wells RE (2005) Subduction zone magnetic anomalies and implications for hydrated forearc mantle. *Geological Society of America Bulletin* 33: 445–448.

b0145 Blakely RJ and Connard GG (1989) Crustal studies using magnetic data. In: Pakiser LC and Mooney WD (eds.) *Geophysical Framework of the Continental United States, Geological Society of America Memoir*, 172, Ch. 4, pp. 45–60. Boulder: Geological Society of America.

b0150 Blakely RJ and Grauch VJS (1983) Magnetic models of crystalline terrane: Accounting for the effect of topography. *Geophysics* 48: 1551–1557.

b0155 Blakely RJ, Jachens RC, Simpson RW, and Couch RW (1985) Tectonic setting of the southern Cascade Range as interpreted from its magnetic and gravity fields. *Geological Society of America Bulletin* 96: 43–48.

b0160 Blakely RJ and Simpson RW (1986) Approximating edges of source bodies from magnetic or gravity anomalies. *Geophysics* 51: 1494–1498.

b0165 Blakely RJ, Wells RE, Tolan TL, Beeson MH, Trehu AM, and Liberty LM (2000) New aeromagnetic data reveal large strike-slip faults in the northern Willamette Valley, Oregon. *Geological Society of America Bulletin* 112: 1225–1233.

b0170 Blakely RJ, Wells RE, Weaver CS, and Johnson SY (2002) Location, structure, and seismicity of the Seattle fault zone, Washington: Evidence from aeromagnetic anomalies, geologic mapping, and seismic-reflection data. *Geological Society of America Bulletin* 114: 169–177.

b0175 Blakely RJ, Wells RE, Yelin TS, Madin IP, and Beeson MH (1995) Tectonic setting of the Portland-Vancouver area, Oregon

and Washington: Constraints from low-altitude aeromagnetic data. *Geological Society of America Bulletin* 107: 1051–1062.

b0180 Bloxham J and Jackson A (1992) Time-dependent mapping of the magnetic field at the core-mantle boundary. *Journal of Geophysical Research* 97: 19537–19563.

b0185 Bosum W, Pucher R, and Roeser H (1985) Crustal anomalies and their causes. In: Fuchs K and Soffel H (eds.) *Geophysics of Solid Earth, the Moon and the Planets*, vol V2, subvolume B, Ch 4.2.1, pp. 74–99. Berlin: Springer.

b0190 Bott MHP (1963) Two methods applicable to computers for evaluating magnetic anomalies due to finite three dimensional bodies. *Geophysical Prospecting* 11: 292–299.

b0195 Bucknam RC, Hemphill-Haley E, and Leopold EB (1992) Abrupt uplift within the past 1700 yr at southern Puget Sound. *Science* 258: 1611–1614.

b0200 Cain JC *et al.* (1974) An N = 22 model of the geomagnetic feld. *EOS, Transaction of the American Geophysical Union* 56: 1108.

AU33

b0205 Cain JC *et al.* (1989) Derivation of a geomagnetic model to n = 63. *Geophysical Journal* 97: 431–441.

b0210 Cady JW (1980) Calculation of gravity and magnetic anomalies of finite-length right polygonal prisms. *Geophysics* 45: 1507–1512.

b0215 Campos-Enriquez JO *et al*. Chicxulub – subsurface structure of impact crater inferred from gravity and magnetic data. *The Leading Edge* 15: 357–359.

AU34

b0220 Caress DW and Parker RL (1989) Spectral interpolation and downward continuation of marine magnetic anomaly data. *Journal of Geophysical Research* 94: 17393–17407.

b0225 Chavez Gomez S (2001) A catalogue of dykes from aeromagnetic surveys in eastern and southern Africa. *ITC Publication # 80*.

b0230 Chenot D and Debeglia N (1990) Three-dimensional gravity or magnetic constrained depth inversion with lateral and vertical variation of contrast. *Geophysics* 55: 327–335.

b0235 Chinese National Aerogeophysics Survey and Remote Sensing Center (1989) *Aeromagnetic Anomaly Map of China and Adjacent Sea, 2nd digital edition in 2004*. Beijing: Geological Publishing House.

b0240 Chulick GS and Mooney WD (2002) Seismic structure of the crust and uppermost mantle of North America and adjacent oceanic basins: A synthesis. *Bulletin of the Seismological Society of America* 92: 2478–2492.

b0245 Clark DA (1997) Magnetic petrophysics and magnetic petrology; aids to geological interpretation of magnetic surveys. *AGSO Journal of Australian Geology and Geophysics* 17: 83–103.

b0250 Clark DA (1999) Magnetic petrology of igneous intrusions: Implications for exploration and magnetic interpretation. *Exploration Geophysics* 30: 5–26.

b0255 Clark SC, Frey H, and Thomas HH (1985) Satellite magnetic anomalies over subduction zones. *Geophysical Research Letters* 12: 41–44.

b0260 Clark DA *et al.* (1998) Remote determination of magnetic properties and improved drill targeting of magnetic anomaly sources by differential vector magnetometry. *Exploration Geophyics* 29: 312–312.

AU34a

b0265 Cohen Y (1989) Traitements et interpretations de donnees spatiales in geomagnetisme: etude des variations laterales d' aimantation de la lithosphere terrestre, *Docteur es sciences physiques thèse*, Paris, 95pp.

b0270 Coleman R (1992) Project magnet high-level vector survey data reduction. In: Langel R and Baldwin R (eds.) *NASA Conference Publication 3153, Types and Characteristics of Data for Geomagnetic field modelling*, pp. 215–248.

AU35

b0275 Constable CG and Parker RL (1988) Smoothing, splines and smoothing splines. *Journal of computational Physics* 78: 493–508.

b0280 Cooper GRJ (2003) Feature detection using sun shading. *Computers and Geosciences* 29: 941–948.

b0285 Cooper GRJ and Cowan DR (2003) Sunshading geophysical data using fractional order horizontal gradients. *The Leading Edge* 22: 204.

b0290 Cordell L (1992) A scattered equivalent-source method for the interpolation and gridding of potential-field data in three dimensions. *Geophysics* 57: 629–636.

b0295 Cordell L and McCafferty AE (1989) A terracing operator for physical property mapping with potential field data. *Geophysics* 54: 621–634.

b0300 Cordell L and Taylor PT (1971) Investigation of magnetization and density of North Atlantic Seamount using Poisson's Theorem. *Geophysics* 36: 919–937.

b0305 Cowan DR and Cooper GRJ (2005) Enhancement of magnetic signatures of impact structures. In: Kenkmann T, Horz F, and Deutsch A (eds.) *Large Meteorite Impacts,* GSA Special Paper 384, pp. 51–65. Geological Society of America.

AU36

b0310 Cowan DR and Cowan S (1993) Separation filtering applied to aeromagnetic data. *Exploration Geophysics* 24: 429–436.

b0315 Craig M (1996) Analytic signals for multivariate data. *Mathematical Geology* 28: 315–329.

b0320 Criss RE and Champion DE (1984) Magnetic properties of granitic rocks from the southern half of the Idaho Batholith: Influences of hydrothermal alteration and implications for aeromagnetic interpretations. *Journal of Geophysical Research* 89: 7061–7076.

b0325 Davies J, Mushayandebvu MF, and Smith R (2004) Magnetic detection and characterization of tertiary and quaternary buried channels. *SEG Expanded Abstracts* 23: 734.

b0330 Dentith M, Cowan D, and Tompkins L (2000) Enhancement of subtle features in aeromagnetic data. *Exploration Geophsics* 31: 104–108.

b0335 Dessler AJ (1986) The evolution of arguments regarding the existence of field-aligned currents. In: Potemra T (ed.) *Magnetospheric Currents*, Geophysical Monograph 28, pp. 22–28. Washington, DC: American Geophysical Union.

b0340 Dimri VP (1998) Fractal behaviour and detectability limits of geophysical surveys. *Geophysics* 63: 1943–1946.

b0345 Dittmer JK and Szymnski JE (1995) The stochastic inversion of magnetics and resistivity data using the simulated annealing algorithm. *Geophysical Prospecting* 43(3): 397–416.

b0350 Dyment J and Arkani-Hamed J (1998) Equivalent sources magnetic dipoles revisited. *Geophysical Research Letters* 25: 2003–2006.

b0355 Dyment J and Arkani-Hamed J (1999) Contibution of lithospheric remanent magnetization to satellite magnetic anomalies over the world's oceans. *Journal of Geophysical Research* 103: 15423–15441.

b0360 Eaton D and Vasudevan K (2004) Skeletonization of aeromagnetic data. *Geophysics* 69: 478–488.

b0365 Elkins-Tanton L and Bowring S (2006) Report on the workshop on the Siberian flood basalts and the end-Permian extinction, NSF-sponsored workshop, Sep 2005.

b0370 Ernst RE *et al.* (1996) Diabase (dolerite) dike swarms of the world: First edition, 1:35,000,000 map, 104pp. *Geological Survey of Canada Open File 3241.*

AU37

b0375 Ernst RE and Buchan KL (1997) Giant radiating dyke swarms: Their use in identifying Pre-Mesozoic large igneous provinces and mantle plumes. In: Mahoney JJ and Coffin MF (eds.) *Large Igneous Provinces: Continental, Oceanic, and Planetary Flood Volcanism,* American Geophysical Union Monograph 100, pp. 297–333. Washington, DC: American Geophysical Union.

b0380 Ernst RE and Buchan KL (2001) The use of mafic dike swarms in identifying and locating mantle plumes. In: Ernst RE and Buchan KL (eds.). *Mantle Plumes: Their Identification Through Time, Geological Society of America Special Paper*

352, pp. 247–265. Boulder CO: Geological Society of America.

b0385 Erwin DE (1994) The Permo-Triassic extinction. *Nature* 367: 231–236.

b0390 Finn C (1990) Geophysical constraints on Washington convergent margin structure. *Journal of Geophysical Research* 95: 19533–19546.

b0395 Fox Maule C, Purucker M, Olsen N, and Mosegaard K (2005) Heat flux anomalies in Antarctica revealed by satellite magnetic data. *Science* 309: 464–467.

b0400 Frost BR (1991a) Magnetic petrology: Factors that control the occurrence of magnetite in crustal rocks. In: Lindsley DH (ed.) *Oxide Minerals: Petrologic and Magnetic Significance*, vol. 25, Ch. 14, pp. 489–509. Blacksburg, VA: Mineralogical Society of America.

b0405 Frost BR (1991b) Stability of oxide minerals in metamorphic rocks. In: Lindsley DH (ed.) *Oxide Minerals: Petrologic and Magnetic Significance*, vol. 25, Ch. 13, pp. 469–488. Blacksburg, VA: Mineralogical Society of America.

b0410 Frost BR (1991c) Introduction to oxygen fugacity and its petrologic importance. In: Lindsley DH (ed.) *Oxide Minerals: Petrologic and Magnetic Significance*, vol. 25, Ch. 1, pp. 1–8. Blacksburg, VA: Mineralogical Society of America.

b0415 Frost BR and Shive PN (1989) Comment on Limiting depth of magnetization in Cratonic Lithosphere. *Geographical Research Letters* 16: 477–479.

b0420 Geological Survey of Canada (1995) Magnetic anomalies and tectonic elements of Northeast Eurasia. GSC Open-File Report 2574.

b0425 Geological Survey of Japan (2002) Magnetic anomaly map of east Asia. *Geological Survey of Japan Digital Geoscience Map P-3,* 2nd edn.

AU38

b0430 Gerovska D and Araúzo-Bravo MJ (2003) Automatic interpretation of magnetic data based on Euler deconvolution with unprescribed structural index. *Computers and Geosciences* 29: 949–960.

b0435 Getech (1996) http://www.getech.com/data.

b0440 Gibson RI (1998) Gravity and magnetics in oil exploration: A historical perspective. In: *Geologic Applications of Gravity and Magnetics: Case Histories, Society of Exploration Geophysics. Geophysical Reference Series 8.* Tulsa, OK.

AU39

b0445 Gibson RI (1998) Interpretation of Rift-stage Faulting in the West Siberian Basin from Magnetic Data. In: Gibson RI and Millegan PS (eds.) *Geologic Applications of Gravity and Magnetics*. Exploration Geophysics Geophysical Reference Series 8, pp. 79–81. Tulsa, OK.

AU40

b0450 Gibson RI and Millegan PS (eds.) (1998) *Geologic Applications of Gravity and Magnetics: Case Histories, Society of Exploration Geophysics Geophysical Reference Series 8:* Tulsa, OK.

AU41

b0455 Girdler RW, Taylor PT, and Frawley JJ (1992) A possible impact origin for the Bangui magnetic anomaly (Central Africa). *Tectonophysics* 212: 45–58.

b0460 Goldhaber MB and Reynolds RL (1991) Relations among hydrocarbon reservoirs, epigenetic sulfidization, and rock magnetization: Examples from the south Texas costal plain. *Geophysics* 56: 748–757.

b0465 Goldstein NE and Ward SH (1966) The separation of remanent from induced magnetism. *in situ. Geophysics* 31: 779–796.

b0470 Golynsky AM, *et al.* (2001) ADMAP – Magnetic anomaly map of the Antarctic, 1:10 000 000 scale map. In: Morris PR and von Frese R (eds.) *BAS (Misc.) 10*, Cambridge: British Antarctic Survey..

AU42

b0475 Goussev SA, Charters RA, Peirce JW, and Glenn WE (2003) The Meter Reader – Jackpine magnetic anomaly: Identification of a buried meteorite impact structure. *The Leading Edge* 22: 740–741.

b0480 Grace JD and Hart GF (1990) Urengoy gas field—USSR West Siberian basin, Tyumen District. In: Beaumont EA and Foster NH (eds.) *Structural Traps III, Tectonic Old and Fault Traps, AAPG Treatise of Petroleum Geology, Atlas of Oil and Gas fields*, A-109, pp. 309–335. Tulsa, Ok.

AU42a

Grant FS (1985) Aeromagnetics, geology and ore environments: b0485
In: Magnetite in igneous, sedimentary and metamorphic rocks: An overview. *Geoexploration* 23: 303–333.

Grant FS and West GF (1965) *Interpretation Theory in Applied* b0490
Geophysics. New York: McGraw-Hill.

Grammatica N and Tarits P (2002) Contribution at satellite alti- b0495
tude of electromagnetically induced anomalies from a three-dimensional heterogeneously conducting Earth, using SQ as an inducing source field. *Geophysical Journal International* 151: 913–923.

Grauch VJS (1987) A new variable-magnetization terrain cor- b0500
rection method for aeromagnetic data. *Geophysics* 52: 94–107.

Grieve R and Therriault A (2000) Vredefort, Sudbury, Chicxulub: b0505
Three of a kind? *Annual Review of Earth and Planetary Science* 28: 305–338.

Gubbins D and Herrero-Bervera E (eds.) (2006) *Encyclopedia of* b0510
Geomagnetism and Paleomagnetism. Berlin: Springer.

Gunn PJ (1975) Linear transformations of gravity and magnetic b0515
fields. *Geophysical Prospecting* 23: 300–312.

Gunn PJ (ed.) (1997) Airborne magnetic and radiometric sur- b0520
veys. *AGSO Journal* 17: 2.

Haggerty SE (1976) Opaque mineral oxides in terrestrial igneous b0525
rocks. In: Rumble D (ed.) *Oxide Minerals*, vol. 3., Ch. 4, pp. 1–98. Blacksburg: Mineralogical Society of America.

Haggerty SE (1979) The aeromagnetic mineralogy of igneous b0530
rocks. *Canadian Journal of Earth Sciences* 16: 1281–1293.

Hahn A, Ahrendt H, Meyer J, and Hufen JH (1984) A model of b0535
magnetic sources within the Earth's crust compatible with the field measured by the satellite Magsat. *Geol. Jb.,* A75: 125–156.

AU43

Hahn A and Bosum W (1986) *Geomagnetics: Selected* b0540
Examples and Case Histories. Berlin: Geopublication Associates.

Hanna WF (ed.) (1987) Geologic applications of modern aero- b0545
magnetic surveys. *USGS Bulletin*, *1924.*

AU44

Hansen RO (1993) Interpretative gridding by anisotropic kriging. b0550
Geophysics 58: 1491–1497.

Hansen RO (2005) 3D multiple-source Werner deconvolution for b0555
magnetic data. *Geophysics* 70: L45–L51.

Hansen RO and Miyazaki Y (1984) Continuation of potential b0560
fields between arbitrary surfaces. *Geophysics* 49: 787–795.

Hansen RO and Pawlowski RS (1989) Reduction to the pole at b0565
low latitudes by Wiener filtering. *Geophysics* 54: 1607–1613.

Hansen RO and Simmonds M (1993) Multiple-source Werner b0570
deconvolution Geophysics 58: 1792–1800.

Hansen RO and Suciu L (2002) Multiple-source Euler deconvo- b0575
lution. *Geophysics* 67: 525–535.

Hansen RO and Wang X (1988) Simplified frequency-domain b0580
expressions for potential fields of arbitrary three-dimensional bodies. *Geophysics* 53: 365–374.

Harrison C (1987) The crustal field. In: Jacobs J (ed.) b0585
Geomagnetism, vol 1, Ch. 5, pp. 513–610. London: Academic Press.

Heirtzler JR, Dickson GO, Herron EM, Pitman WC, and Le b0590
Pichon X (1968) Marine magnetic anomalies, geomagnetic field reversals, and motions of the ocean floor and continents. *Journal of Geophysical Research* 73: 2119–2136.

Hemant K and Maus S (2006) Geological modeling of the new b0595
CHAMP magnetic anomaly maps using a Geophysical Information System (GIS) technique. *Journal of Geophysical Research* .

AU45

Hemant K and Maus S (2005) Why no anomaly is visible over b0600
most of the continent-ocean boundary in the global crustal magnetic field. *Physics of the Earth and Planetary Interiors* 149: 321–333.

b0605 Hernandez I *et al.* (2001) Aeromagnetic map of Mexico: An exploration approach for the new millennium —A progress report. *Revista Geofisica Instituto Panamericano de Geografia e Historia* 55, 33pp.

b0610 Hildebrand AR, *et al.* (1991) Chicxulub crater: A possible Cretaceous–Tertiary boundary impact crater on the Yucatan peninsula. *Geology* 19: 867–871.

b0615 Hill PL (1986) Bibliographies and location maps of aeromagnetic and aeroradio metric publications for the United States. *US Geological Survey Open-File Report 86-525*, Reston, Virginia.

b0620 Hinze W (1979) Continental magnetic anomalies. *Reviews of Geophysics and Space Physics* 17: 257–273.

b0625 Hinze W, *et al.* (1988) Magnetic anomaly map of North America. *The Leading Edge* 7: 19–21.

b0630 Hinze W, Von Frese R, and Ravat D (1991) Mean magnetic contrast between oceans and continents. *Tectonophysics* 192: 117–127.

b0635 Hinze WJ (ed.) (1985) *The Utility of Regional Gravity and Magnetic Anomaly Maps*. Tulsa, OK: Society of Exploration Geophysicists.

b0640 Hinze WJ and Zietz I (1985) The composite magnetic-anomaly map of the conterminous United States. In: Hinze WJ (ed.) *The Utility of Regional Gravity and Magnetic Anomaly Maps*, pp. 1–24. Tulsa, OK: Society of Exploration Geophysicists.

b0645 Hitzman MW, Oreskes N, and Einaudi MT (1992) Geological characteristics and tectonic setting of Proterozoic iron oxide (Cu–U–Au–REE) deposits. *Precambrian Research* 58: 241–287.

b0650 Hood PJ, McGrath PH, and Teskey DJ (1985) Evolution of Geological Survey of Canada magnetic-anomaly maps. A Canadian perspective. In: Hinze WJ (ed.) *The Utility of Regional Gravity and Magnetic Anomaly Maps*, pp. 62–87. Tulsa, OK: Society of Exploration Geophysicists.

b0655 Hornby P, Boschetti F, and Horowitz FG (1999) Analysis of potential field data in the wavelet domain. *Geophysical Journal International* 137: 175–196.

b0665 Hsu S-K, Coppens D, and Shyu C-T (1998) Depth to magnetic source using the generalized analytic signal. *Geophysics* 63: 1947–1957.

b0660 Hsu S-K, Sibuet J-C, and Shyu C-T (1996) High-resolution detection of geologic boundaries from potential-field anomalies: An enhanced analytic signal technique. *Geophysics* 61: 373–386.

b0670 Hyndman RD and Peacock SM (2003) Serpentinization of the forearc mantle. *Earth and Planetary Science Letters* 212: 417–432.

b0675 Ishihara S (1981) The granitoid series and mineralization. *Economic Geology 75th Anniversary Issue* 458–484.

b0680 Ishihara T (2004) Application of CM3 model in compilation of marine magnetic anomaly data of North Pacific. *Transactions of the American Geophysical Union* 85(47): Fall Meeting Supplement Abstract GP11D-0882.

b0685 Jackson A (1990) Accounting for crustal magnetization in models of the core magnetic field. *Geophysical Journal International* 103: 657–673.

b0690 Jackson A (1994) Statistical treatment of crustal magnetization. *Geophysical Journal International* 119: 991–998.

b0695 Jackson A (1996) Bounding the long wavelength crustal magnetic field. *Physics of the Earth and Planetary Interiors* 98: 283–302.

b0700 Jackson DD (1972) Interpretation of inaccurate, insufficient and inconsistent data. *Geophysical Journal of Royal Astronomical Society* 28: 97–109.

b0705 Jansen J and Witherly K (2004) The Tli Kwi Cho Kimberlite Complex, Northwest Territories, Canada: A Geophysical Case Study. *Society of Exploration of Geophysics 74st Annual Mtg Tech Prog* (Ext. Abstr), Denver, CO. 23: 1147–1149.

Jessell MW (2001) Three-dimensional modeling of potential-field data. *Computers and Geosciences* 27: 455–465. b0710

Jessell MW, and Fractal Geophysics Pty Ltd (2002) An atlas of structural geophysics II. *Journal of the Virtual Explorer* 5 available online at http://www.mssu.edu/seg-vm/exhibits/structuralatlas. b0715

Jonson SY, *et al.* (1996) The southern Whidbey Island fault: An active structure in the Puget Lowland. *Geological Society of America Bulletin* 108: 334–354. b0720

Johnson SY, Dadisman SV, Mosher DC, Blakely RJ, and Childs JR (2001) Active tectonics of the Devils Mountain fault and related structures, northern Puget Lowland and eastern Strait of Juan de Fuca region, Pacific Northwest. *US Geological Survey Professional Paper 1643,* 45pp, 2 plates. b0725

Jourdan F, Fraud G, Bertrand H, Watkeys MK, Kampunzu AB, and Le Gall B (2006) Basement control on dyke distribution in Large Igneous Provinces: Case study of the Karoo triple junction. *Earth and Planetary Science Letters* 241: 307–322. b0730

Kanasewich and Agarwal ER (1970) Analysis of combined gravity and magnetic fields in wavenumber domain. *Journal of Geophysical Research* 75: 5702–5712. b0735 AU50

Keating P (1993) The fractal dimension of gravity data sets and its implication for gridding. *Geophysical Prospecting* 41: 983–994. b0740

Keating P (1995) A simple technique to identify magnetic anomalies due to kimberlite pipes. *Exploration Mining Geology* 4: 121–125. b0745

Keating P and Sailhac P (2004) Use of the analytic signal to identify magnetic anomalies due to kimberlite pipes. *Geophysics* 69: 180–190. b0750

Keating P and Zerbo L (1996) An improved technique for reduction-to-the pole at low latitudes. *Geophysics* 61: 131–137. b0755

Keller GR (1988) The development of gravity and magnetic studies, emphasizing articles published in the GSA Bulletin. *Geological Society of America Bulletin* 100: 469–478. b0760

Kellogg OD (1953) *Foundations of Potential Theory.* Dover. b0765 AU51

Korhonen, *et al.* (1993) One hundred seventy eight thousand petrophysical parameter determinations from the regional Petrophysical Programme. In: Autio S (ed.) *Geological Survey of Finland, Current Research 1991–1992* Geological Survey of Finland. Special Paper 18, pp. 137–141. b0770 AU52 AU53

Koulomzine T, Lamontagne Y, and Nadeau A (1970) New methods for the direct interpretation of magnetic anomalies caused by inclined dikes of infinite length. *Geophysics* 35: 812–830. b0775

Krajick K (2001) *Barren Lands: An Epic Search for Diamonds in the North American Arctic*. New York: Henry Hold. b0780

Ku CC and Sharp JA (1983) Werner deconvolution for automated magnetic interpretation and its refinement using Marquardt inverse modeling. *Geophysics* 48: 754–774. b0785

LaBrecque JL and Ghidella ME (1997) Depth of magnetic basement, and sediment thickness estimates from aero-geophysical data over the western Weddell Basin. *Journal of Geophysical Research* 102: 7929–7945. b0790

LaBrecque JL and Raymond CA (1985) Seafloor spreading anomalies in the MAGSAT field of the North Atlantic. *Journal of Geophycisal Research* 90: 2565–2575. b0795

Langel R and Benson BV (1987) The Magsat bibliography. *NASA Tech Memo.* TM 87822. b0800 AU54

Langel R and Hinze W (1998) *The Magnetic Field of the Earth's Lithosphere*. Cambridge: Cambridge University Press. b0805

Langel RA, *et al.* (1993) The equatorial electrojet and associated currents as seen in the Magsat data. *Journal of Atmospheric and Terrestrial Physics* 55: 1233–1269. b0810 AU55

Langel RA, *et al.* (1996) The near-Earth magnetic field from magnetospheric and quiet-day ionospheric sources and b0815

how it is modelled. *Physics of the Earth and Planetary Interiors* 98: 235–267.

b0820 Langel RA and Estes RH (1982) A geomagnetic filed spectrum. *Geophysical Research Letters* 9: 250–253.

b0825 Langel RA, Slud VE, and Smith PJ (1984) Reduction of satellite magnetic anomaly data. *Journal of Geophysics* 54: 207–212.

b0830 Langlais B, Purucker M, and Mandea M (2004) Crustal magnetic field of Mars. *Journal of Geophysical Research* 109: E02008 doi:10.1029/2033JE002048.

b0835 Leaman DE (1994) Criteria for evaluation of potential field interpretations. *First Break* 12: 181–191.

b0840 LeSchack LA and Van Alstine DR (2002) High-resolution ground-magnetic (HRGM) and radiometric surveys for hydrocarbon exploration: Six case histories in Western Canada. In: Schumacher D and LeSchack LA (eds.) *Surface Exploration Case Histories: Applications of Geochemistry, Magnetics, and Remote Sensing.* AAPG Studies in Geology No. 48 and SEG Geophysical Reference Series No. 11, pp. 67–156. Tulsa, Ok.

b0845 Lesur V and Gubbins D (1999) Evaluation of fast spherical transforms for geophysical applications. *Geophysical Journal Internationl* 139: 547–555.

b0850 Lesur V and Gubbins D (2000) Using geomagnetic secular variation to separate remanent and induced sources of the crustal magnetic field. *Geophysical Journal International* 142: 889–897.

b0855 Lesur V and Maus S (2006) A global lithospheric magnetic field model with reduced noise in the Ploar regions. *Geophysical Research Letters* 33: doi:10.1029/2006GL025826.

b0860 Li X (2003) On the use of different methods for estimating magnetic depth. *The Leading Edge* 22: 1090–1099.

b0865 Li Y and Oldenburg DW (1996) 3-D inversion of magnetic data. *Geophysics* 61: 394–408.

b0870 Li Y and Oldenburg DW (2003) Fast inversion of large-scale magnetic data using wavelet transforms and logarithmic barrier method. *Geophysical Journal International* 152: 251–265.

b0875 Lühr H, Maus S, and Rother M (2004) Noon-time equatorial electrojet: Its spatial features as determined by the CHAMP satellite. *Journal of Geophysical Research* 109: A01306, doi:10.1029/2002JA009656.

b0880 Lindsley DH (ed.) (1991) *Oxide Minerals: Petrologic and Magnetic Significance, vol. 25.* Blacksburg, VA: Mineralogical Society of America.

b0885 Lowe DAJ, Parker RL, Purucker ME, and Constable CG (2001) Estimating the crustal power spectrum from vector Magsat data. *Journal of Geophysical Research* 106: 8589–8598.

b0890 Machel HG and Burton EA (1991) Chemical and microbial processes causing anomalous magnetization in environments affected by hydrocarbon seepage. *Geophysics* 56: 598–605.

b0895 Macnae JC (1979) Kimberlites and exploration geophysics. *Geophysics* 44: 1395–1416.

b0900 Macnab R, *et al.* (1995) New database documents the magnetic character of the Arctic and North Atlantic. *EOS, Transactions of the American Geophysical Union* 76(45): 449–458.

b0905 Makarova ZA (ed.) (1974) Map of the anomalous magnetic field of the Territory of the USSR and adjacent marine areas, scale 1:2,500,000 (18 sheets). *USSR Ministry of Geology*. Leningrad: VSEGEI.

b0910 Malin SRC, Duzgit Z, and Baydemir N (1996) Rectangular harmonic analysis revisited. *Journal of Geophysical Research* 101: 28205–28209.

b0915 Mandea M and Langlais B (2002) Observatory crustal magnetic biases during MAGSAT and Orsted satellite missions. *Geophysical Research Letters* 29: http://dx.doi.org/10.1029/2001GL013693.

b0920 Mandea M and Purucker M (2005) Observing, modeling, and interpreting magnetic fields of the solid Earth. *Surveys in Geophysics* http://dx.doi.org/10.1007/s10712-005-3857-x.

Marsh JS (2005) DISCUSSION: The geophysical mapping of Mesozoic dyke swarms in southern Africa and their origin in the disruption of Gondwana. *Journal of African Earth Sciences* 35: 525–527. b0925

Maus S, *et al.* (2006) Earth's lithospheric magnetic field determined to spherical harmonic degree 90 from CHAMP satellite measurements. *Geophysical Journal International* 164: 319–330. b0930

b0935 Maus S and Dimri VP (1996) Depth estimation from the scaling power spectrum of potential fields? *Geophysical Journal International* 124: 113–120.

b0940 Maus S, Gordon D, and Fairhead JD (1997) Curie temperature depth estimation using a self-similar magnetisation model. *Geophysical Journal International* 129: 163–168.

b0945 Maus S and Haak V (2002) Is the long wavelength crustal magnetic field dominated by induced or by remanent magnetisation? *Journal of Indian Geophysical Union* 6: 1–5.

b0950 Maus S and Haak V (2003) Magnetic field annihilators: Invisible magnetisation at the magnetic equator. *Geophysical Journal International* 155: 509–513.

b0955 Maus S and Macmillan S (2005) 10th generation international geomagnetic reference field. *EOS Transactions of the American Geophysical Union* 86: 159.

b0960 May PR (1971) Pattern of Triassic–Jurassic diabase dyks around the North Atlantic in context of predrift position of the continents. *Geological Society of America Bulletin* 82: 1285–1292.

b0965 Mayhew M (1982) Application of satellite magnetic anomaly data to Curie isotherm mapping. *Journal of Geophysical Research* 87: 4846–4854.

b0970 Mayhew M and Estes R (1983) Equivalent source modeling of the core magnetic field using Magsat data. *Journal of Geomagnetism and Geoelectricity* 35: 119–130.

b0975 Mayhew M and Johnson BD (1987) An equivalent layer magnetization model for Australia based on Magsat data. *Earth and Planetary Science Letters* 83: 167–174.

b0980 Mayhew M, Johnson BD, and Wasilewski PJ (1985) A review of problems and progress in studies of satellite magnetic anomalies. *Journal of Geophysical Research* 90: 2511–2522.

b0985 Mayhew M and LaBrecque J (1987) Crustal geologic studies with Magsat and surface magnetic data. *Reviews of Geophysics* 25: 971–981.

b0990 McEnroe SA, *et al.* (2001) Effect of fine-scale microstructures in titanohematite on the acquisition and stability of natural remanent magnetization in granulite facies metamorphic rocks, southwest Sweden: Implications for crustal magnetism. *Journal of Geophysical Research* 106: 30523–30546.

b0995 McEnroe SA, Robinson P, and Panish P (2001) Aeromagnetic anomalies, magnetic petrology and rock magnetism of hemo-ilmenite-and magnetite-rich cumulates from the Sokndal Region, South Rogaland, Norway. *American Mineralogist* 86: 1447–1468.

b1000 McEnroe SA and Brown LL (2000) A closer look at remanence-dominated anomalies: Rock-magnetic properties and magnetic mineralogy of the Russell Belt microcline-sillmanite gneisses, Northwest Adirondacks Mountains, New York. *Journal of Geophysical Research* 105: 16,437–16,456.

b1005 McLeod MG (1996) Spatial and temporal power spectra of the geomagnetic field. *Journal of Geophysical Research* 101: 2745–2763.

b1010 Meissner R (1986) *The Continental Crust-A Geophysical Approach,* International Geophysics Series 34. San Diego, CA: Academic.

b1015 Milligan PR, *et al.* (2005) Fourth edition Magnetic Anomaly Map of Australia, derived from a new-generation Magnetic Anomaly Grid Database of Australia (MAGDA), International Association of Geomagnetism Aeronomy, IAGA2005-A-01186, Toulouse, France.

b1020 Miligan PR and Franklin R (2004) Magnetic anomaly map of Australia, Geoscience Australia, 1:25000000.

b1025 Modisi MP, Atekwana EA, Kampunzu AB, and Ngwisanyi TH (2000) Rift kinematics during the incipient stages of continental extension: Evidence from the nascent Okavango rift basin, northwest Botswana. *Geology* 28: 939–942.

b1030 Mooney WD, Laske G, and Masters TG (1998) Crust 5.1: A global crustal model at 5×5. *Journal of Geophysical Research* 103: 727–748.

b1035 Moreau F, Gibert D, Holschneider M, and Saracco G (1997) Wavelet analysis of potential fields. *Inverse Problems* 13: 165–178.

b1040 Mosegaard K and Sambridge M (2002) Monte Carlo analysis of Inverse Problems. *Inverse Problems* 18: R29–R54.

b1045 Mubu MS (1995) *Aeromagnetic Mapping and Interpretation of Mafic Dyke Swarms in Southern Africa.* MSc Thesis, ITC Delft, Netherlands, 63pp.

b1050 Mushayandebvu MF, Lesur V, Reid AB, and Fairhead JD (2004) Grid Euler deconvolution with constraints for 2D structures. *Geophysics* 69: 489–496.

b1055 Mushayandebvu MF, van Driel P, Reid AB, and Fairhead JD (2001) Magnetic source parameters of two-dimensional structures using extended Euler deconvolution. *Geophysics* 66: 814–823.

b1060 Nabighian MN (1972) The analytic signal of two-dimensional magnetic bodies with polygonal cross-section: Its properties and use for automated interpretation. *Geophysics* 37: 507–517.

b1065 Nabighian MN (1984) Toward a three-dimensional automatic interpretation of potential field data via generalized Hilbert transforms: Fundamental relations. *Geophysics* 49: 780–786.

b1070 Nabighian MN, *et al.* (2005) The historical development of the magnetic method in exploration. *Geophysics* 70: 33–61. AU61

b1075 Nabighian MN and Asten MW (2002) Metalliferous mining geophysics-State of the art in the last decade of the century and the beginning of the new millennium. *Geophysics* 67: 964–978.

b1080 Nabighian MN and Hansen RO (2001) Unification of Euler and Werner deconvolution in three dimensions via the generalized Hilbert transform. *Geophysics* 66: 1805–1810.

b1085 Nakagawa I and Yukutake T (1985) Rectangular harmonic analysis of geomagnetic anomalies derived from Magsat data over the area of the Japanese islands. *Journal of Geomagnetisn and Geolectricity* 37: 957–977.

b1090 Naidu PS (1970) Fourier transform of large scale aeromagnetic field using a modified version of Fast Fourier Transform. *Pure and Applied Geophysics* 81: 17–25.

b1095 Nataf H and Ricard Y (1996) An a priori tomographic model of the upper mantle based on geophysical modeling. *Physics of the Earth and Planetary Interiors* 95: 101–122.

b1100 Naudy H (1971) Automatic determination of depth on aeromagnetic profiles. *Geophysics* 36: 717–722.

b1105 Nelson JB (1988) Calculation of the magnetic gradient tensor from total field gradient measurements and its application to geophysical interpretation. *Geophysics* 53: 957–966.

b1110 NGDC (1996) Magnetic anomaly data of the former USSR, US Naval Oceanographic Office, in collaboration with the Ministry of Geology of the USSR, 1 CD-ROM.

b1115 O'Brien MS and Parker RL (1994) Regularized geomagnetic field modeling using monoples. *Geophysical Journal International* 118: 566–578.

b1120 O'Connell MD, *et al.* (2005) Gridding aeromagnetic data using longitudinal and transverse gradients with the minimum curvature operator. *The Leading Edge* 24: 142–145. AU62

b1125 Olsen N, Lühr H, Sabaka TJ, *et al.* (2006a) CHAOS-A model of Earth's magnetic field derived from CHAMP, Orsted, and SAC-C magnetic field data. *Geophysical Journal International* 166: 67–75.

b1130 Olsen N, *et al.* (2006b) The Swarm end-to-end mission simulator study: A demonstration of separating the various contributions to Earth's magnetic field using synthetic data. *Earth Planets Space* 58: 359–370. AU63

Parker RL (1972) Inverse theory with grossly inadequate data. b1140 *Geophysical Journal of Royal Astronomical Society* 29: 123–138.

Parker RL (1973) The rapid calculation of potential anomalies. b1145 *Geophysical Journal of Royal Astronomical Society* 31: 447–455.

Parker RL (1974) Best bounds on density and depth from gravity b1150 data. *Geophysics* 39: 644–649.

Parker RL (1975) The theory of ideal bodies for gravity inter- b1155 pretation. *Geophysical Journal of Royal Astronomical Society* 42: 315–334.

Parker RL (1986) Harmonic splines in geomagnetism, in b1160 *Function Estimation*. *American Mathematical Society Proceedings of Contemporary Mathematics* 59: 63–76. AU64

Parker RL (1988) A statistical theory of seamount magnetism. b1165 *Journal of Geophysical Research* 93: 3105–3115.

Parker RL (1991) A theory of ideal bodies for seamount mag- b1170 netism. *Journal of Geophysical Research* 96: 16101–16112.

Parker RL (1997) Coherence of signals from magnetometers on b1175 parallel paths. *Journal of Geophysical Research* 102: 5111–5117.

Parker RL (2003) Ideal bodies for Mars magnetics. *Journal of* b1180 *Geophysical Research* 108: E1 5006, doi: 10.1029/2001JE001760.

Parker RL and Huestis SP (1974) Inversion of magnetic b1185 anomalies in the presence of topography. *Journal of Geophysical Research* 79: 1587–1593.

Parker RL and Klitgord KD (1972) Magnetic upward continua- b1190 tion from an uneven track. *Geophysics* 37: 662–668.

Parker RL and O'Brien MS (1997) Spectral analysis of vector b1135 magnetic field profiles. *Journal of Geophysical Research* 102: 24815–24822.

Parker RL and Shure L (1982) Efficient modeling of the Earth's b1195 magnetic field with harmonic splines. *Geophysical Research Letters* 9: 812–815.

Parker RL and Shure L (1985) Gravitational and magnetic fields b1200 of some simple solids of revolution. *Geophysical Journal of Royal Astronomical Society* 80: 631–647.

Parker RL, Shure L, and Hildebrand J (1987) The application of b1205 inverse theory to seamount magnetism. *Reviews of Geophysics* 25: 17–40.

Paterson NR and Reeves CV (1985) Applications of gravity and b1210 magnetic surveys: The state-of-the-art in 1985. *Geophysics* 50: 2558–2594.

Pedersen LB (1977) Interpretation of potential field data- b1215 A generalized inverse approach. *Geophysical Prospecting* 25: 199–230.

Pedersen LB (1978) Wavenumber domain expressions for b1220 potential fields from arbitrary 2-, $2^1/2$-, and 3-dimensional bodies. *Geophysics* 43: 626–630.

Pedersen LB (1979) Constrained inversion of potential field b1225 data. *Geophysical Prospecting* 27: 726–748.

Pedersen LB (1991) Relations between potential fields and b1230 some equivalent sources. *Geophysics* 56: 961–971.

Pedersen LB and Rasmussen TM (1990) The gradient tensor of b1235 potential field anomalies: Some implications on data collection and data processing of maps. *Geophysics* 55: 1558–1566.

Penfield GT and Camargo ZA (1981) Definition of a major b1240 igneous zone in the central Yucatan with aeromagnetics and gravity. *Society of Exploration Geophysics 51st Annual Mtg Tech Prog* (Abstr), 37 Los Angeles, CA.

Peters LJ (1949) The direct approach to magnetic interpretation b1245 and its practial application. *Geophysics* 14: 290–320.

Phillips JD (1997) Potential-field geophysical software for the b1250 PC-version 2.2. *US Geological Surver Open-File Report 97-725*, 34 pp.

b1255 Phillips JD, Reynolds RL, and Frey H (1991) Crustal structure interpreted from magnetic anomalies. *Reviews of Geophysics Supplement* 416–427.
AU65
b1260 Pilkington M (1997) 3-D magnetic imaging using conjugate gradients *Geophysics* 62: 1132–1142.
b1265 Pilkington M and Crossley DJ (1986) Determination of crustal interface topography from potential fields. *Geophysics* 51: 1277–1284.
b1270 Pilkington M and Grieve RAF (1992) The geophysical signature of terrestrial impact craters. *Reviews of Geophysics* 30: 161–181.
b1275 Pilkington M and Hildebrand AR (2000) Three-dimensional magnetic imaging of the Chicxulub crater. *Journal of Geophysical Research* 105: 23,479–23,491.
b1280 Pilkington M and Keating P (2004) Contact mapping from gridded magnetic data – A comparison of techniques. *Exploration Geophysics* 35: 306–311.
b1285 Pilkington M and Todoeschuck JP (1995) Scaling nature of crustal susceptibilities. *Geophysical Research Letters* 22: 779–782.
b1290 Plouff D (1976) Gravity and magnetic fields of polygonal prisms and application to magnetic terrain corrections. *Geophysics* 41: 727–741.
b1295 Power M, Belcourt G, and Rockel E (2004) Geophysical methods for kimberlite exploration in northern Canada. *The Leading Edge* 23: 1124–1129.
b1300 Press WH, Teukolsky SA, Vetterling WT, and Flannery BP (1992) Numerical Recipes in Fortran. *The Art of Scientific Computing,* 2nd edn. Cambridge: Cambridge Press.
b1305 Press WH, Teukolsky SA, Vetterling WT, and Flannery BP (1996) Numerical Recipes in Fortran 90. *The Art of Scientific Computing*. Cambridge: Cambridge Press.
b1310 Press WH, Teukolsky SA, Vetterling WT, and Flannery BP (1997) Numerical Recipes in C. *The Art of Scientific Computing,* 2nd edn. Cambridge: Cambridge Press.
b1315 Prieto C and Morton G (2003) New insights from a 3D Earth model, deepwater Gulf of Mexico. *The Leading Edge* 22: 356–366.
b1320 Primdahl F (2000) Resonance magnetometers. In: Ripka P (ed.), *Magnetic Sensors and Magnetometers*, pp. 267–304. Boston: Artech.
b1325 Purucker M (1990) The Computation of vector magnetic anomalies: A comparison of techniques and errors. *Physics of the Earth and Planetary Interiors* 62: 231–245.
b1330 Purucker M and Ishihara T (2005) Magnetic images of the Sumatran region crust. *EOS Transactions of the American Geophysical Union* 86(10): 101–102.
b1335 Purucker M, Langel R, Rajaram M, and Raymond C (1998) Global magnetization models with *a priori* information *Journal of Geophysical Research* 103: 2563–2584.
b1340 Purucker M, Langlais B, Olsen N, Hulot G, and Mandea M (2002) The southern edge of crationic North America: Evidence from new satellite magnetometer observations. *Geophysical Research Letters* 29(15): 8000 doi:10.1029/2001GL013645.
b1345 Purucker M and Mandea M (2005) New research directions based on the World Digital Magnetic Anomaly Map, and Swarm, International Association Geomagnetism of Aeronomy International Meeting, Toulouse, France, 18–29 Jul. 2005.
b1350 Purucker M, Sabaka T, and Langel R (1996) Conjugate gradient analysis: A new tool for studying satellite magnetic data sets. *Geophysical Research Letters* 23: 507–510.
b1355 Purucker M, Von Frese RRB, and Taylor PT (1999) Mapping and interpretation of satellite magnetic anomalies from POGO data over the Antarctic region. *Annali Di Geofisica* 42: 215–228.
b1360 Purucker M and Whaler K (2003) Merging satellite and aeromagnetic data over Europe, the North Atlantic, and the Arctic, 2nd CHAMP Science meeting, 1–4 Sep 2003, Potsdam, Germany.
Purucker M and Whaler K (2004) Recognizing and interpreting b1365
the longest wavelength lithospheric magnetic fields obscured by overlap with the core field. *Eos Transactions of the American Geophysical Union* 85(47): Fall Meeting Supplement Abstract GP31A-0821.
Rasmussen R and Pedersen LB (1979) End corrections in b1370
potential field modeling. *Geophysical Prospecting* 27: 749–760.
Ravat D (1996) Analysis of the Euler method and its applicability b1375
in environmental magnetic applications. *Journal of Environmental Engineering and Geophysics* 1: 229–238.
Ravat D, Hildenbrand TG, and Roest W (2003) New way of b1380
processing near-suface magnetic data: The utillty of the comprehensive model of the magnetic field. *The Leading Edge* 22: 784–785.
Ravat D, Whaler K, Pilkington M, Sabaka T, and Purucker M b1385
(2002) Compatibility of high-altitude aeromagnetic and satellite altitude magnetic anomalies over Canada. *Geophysics* 67: 546–554.
Ray RD (1985) Correction of systematic error in magnetic sur- b1390
veys: An application of ridge regression and sparse matrix theory. *Geophysics* 50: 1721–1731.
Reeves CV (2000) The geophysical mapping of Mesozoic b1395
dyke swarms in southern Africa and their origin in the disruption of Gondwana. *Journal of African Earth Sciences* 30: 499–513.
Reeves CV and Erren H (1994) AAIME: Aeromagnetics of b1400
Arabia, India, and the Middle East. *International Institute for Aerospace Survey and Earth Science* (unpublished).
AU66
Reeves CV, Macnab R, and Maschenkov S (1998) Compiling all b1405
world' magnetic anomalies. *Eos Transactions of the American Geophysical Union* 79(28): 338–339.
Reford S (2006) Gradient enhancement of the total magnetic b1410
field. *The Leading Edge* 25: 59–66.
Reichow MK, *et al.* (2002) Ar–Ar Dates from the West Siberian b1415
Basin: Siberian Flood Basalt Province Doubled. *Science* 296: 1846–1849.
AU67
Reid AB (1980) Aeromagnetic surver design. *Geophysics* b1420
45: 973–976.
Reid AB, Allsop JM, Granser H, Millett AJ, and Somerton IW b1425
(1990) Magnetic interpretation in three dimensions using Euler deconvolution. *Geophysics* 55: 80–91.
Reynolds RL, *et al.* (1990a) Iron sulphide minerals at Cement b1430
oilfield, Oklahoma: Implications for magnetic detection of oilfields. *Geological Society of America Bulletin* 102: 368–380.
AU68
Reynolds RL, *et al.* (1990b) Magnetic forward models of Cement b1435
oil field, Oklahoma based on rock magnetic, geochemical and petrological constraints. *Geophysics* 55: 344–353.
AU69
Reynolds RL, *et al.* (1990c) Rock magnetism, the distribution of b1440
magnetic minerals in the Earth's crust, and aeromagnetic anomalies. In: Hanna WF (ed.) *Geologic Applications of Modern Aeromagnetic Surveys*, pp. 24–45. Denver, CO: US Geological Survery Bulletin 1924.
AU70
Reynolds RL, *et al.* (1994) Magnetization and geochemistry of b1450
greigite-bearing Cretaceous strata, North Slope Basin, Alaska. *American Journal of Science* 294: 485–528.
Reynolds RL, Fishman NS, and Hudson MR (1991) Sources of b1445
aeromagnetic anomalies over Cement oil field (Oklahoma), Simpson oil field (Alaska), and the wyoming-Idaho-Utah thrust belt. *Geophysics* 56: 606–627.
Ridsdill-Smith TA and Dentith MC (1999) The wavelet transform b1455
in aeromagnetic processing. *Geophysics* 64: 1003–1013.
Rigoti A, Padilha AL, Chamalaun FH, and Trivedi NB (2000) b1460
Effects of the equatorial electrojet on aeromagnetic data acquisition. *Geophysics* 65: 553–558.
Ripka P (2000) Fluxgate magnetometers. In: Ripka P (ed.) b1465
Magnetic Sensors and Magnetometers, pp. 75–128. Boston: Artech.

b1470 Roest WR and Pilkington M (1993) Identifying remanent magnetization effects in magnetic data. *Geophysics* 58: 653–659.
b1475 Roest WR, Verhoef J, and Pilkington M (1992) Magnetic interpretation using the 3-D analytic signal. *Geophysics* 57: 116–125.
b1480 Runcorn SK (1975) On the interpretation of lunar magnetism. 10: 327–335.
b1485 Rygaard-Hjalsted C, Mosegaard K, and Olsen N (2000) Resolution studies of fluid flow models near the core–mantle boundary through Bayesian inversion of geomagnetic data. In: Hansen PC, Jacobsen BH, and Mosegaard K (eds.) *Methods and Applications of Inversion: Proceeding of IIC98 conference (Copenhagen, 1998)* pp. 255–275.
b1490 Saad AH (1969) Magnetic properties of ultramafic rocks from Red Mountain, California. *Geophysics* 34: 974–987.
b1495 Sabaka TJ, Olsen N, and Langel RA (2002) A comprehensive model of the quiet-time, near-the-Earth magnetic field: Phase 3. *Geophysical Journal International* 151: 32–68.
b1500 Sabaka TJ, Olsen N, and Purucker ME (2004) Extending comprehensive models of the Earth's magnetic field with Orsted and Champ data. *Geophysical Journal International* 159: 521–547.
b1505 Sailhac P, Galdeano A, Gibert D, Moreau F, and Delor C (2000) Identification of sources of potential fields with the continuous wavelet transform: Complex wavelets and application to aeromagnetic profiles in French Guiana. *Journal of Geophysical Research* 105: 19455–19475.
b1510 Salem A and Ravat D (2003) A combined analytic signal and Euler method (AN-EUL) for automatic interpretation of magnetic data. *Geophysics* 68: 1952–1961.
b1515 Saltus RW, *et al.* (2005) Utility of aeromagnetic studies for mapping of potentially active faults in two forearc basins: Puget Sound, Washington, and Cook Inlet, Alaska. *Earth Planets Space* 57: 781–793.
b1520 Sambridge M and Mosegaard K (2002) Monte Carlo methods in geophysical inverse problems. *Review of Geophysics* 40: 1009 doi: 10.1029/200RG0089.
b1525 Schlinger CM (1985) Magnetization of lower crust and interpretation of regional magnetic anomalies-Example from Lofoten and Vesteraen, Norway. *Journal of Geophysical Research* 90: 1484–1504.
b1530 Schnetzler CC and Taylor PT (1984) Evaluation of an observational method for estimation of remanent magnetization. *Geophysics* 49: 282–290.
b1535 Schnetzler CC, Taylor PT, Langel RA, Hinze WJ, and Phillips JD (1985) Comparison between the recent US composite magnetic anomaly map and Magsat anomaly data. *Journal of Geophysical Research* 90: 2543–2548.
b1540 Sexton MA, *et al.* (1995) The Mt. Leyshon magnetic anomaly. *Exploration Geophysics* 26: 84–91.
b1545 Shah AK, *et al.* (2005) New surveys of the Chesapeake Bay impact structure suggest melt pockets and target-structure effect. *Geology* 33: 417–420.
b1550 Sharpton VL, *et al.* (1992) New links between the Chicxulub impact structure and the Cretaceous/Tertiary boundary. *Nature* 359: 819–821.
b1555 Shive PN, *et al.* (1992) Magnetic properties of the lower crust. In: Fountain DM, Arculus R, and Kay RW (eds.) *Continental Lower Crust, Developments in Geotectonics 23*, pp. 145–178. New York: Elsevier.
b1560 Shure L, Parker RL, and Backus GE (1982) Harmonic splines for geomagnetic modelling. *Physics of the Earth and Planetary Interiors* 28: 215–229.
b1565 Siebert M and Meyer J (1996) Geomagnetic activity indices. In: Dieminger W, Hartmann GK, and Leitinger R (eds.) *The Upper Atmosphere: Data Analysis and Interpretation*, Ch. V.3, pp. 887–911. Berlin: Springer.
Silva JBC (1986) Reduction to the pole as an inverse problem and its application to low-latitude anomalies. *Geophysics* 51: 369–382. b1570
Silva JBC and Barbosa VCF (2003) 3D Euler deconvolution: Theoretical basis for automatically selecting good solutions. *Geophysics* 68: 1962–1968. b1580
Silva JBC, Barbosa VCF, and Medeiros WE (2001) Scattering, symmetry, and bias analysis of source position estimates in Euler deconvolution and its practical implications. *Geophysics* 66: 1149–1156. b1575
Shive PN, *et al.* (1992) Magnetic properties of the lower continental crust. In: Fountain DM, Arculus R, and Kay RW (eds.) *Continental Lower Crust: Developments in Geotectonics 23*, pp. 145–177. Amsterdam: Elsevier. b1585
Sleep NH (2005) Evolution of the continental lithosphere. *Annual Review of Earth and Planetary Sciences* 33: 369–393. b1590
Smith WHF and Wessel P (1990) Griding with continuous curvature splines in tension. *Geophysics* 55: 293–305. b1595
Snyder DB, Hobbs RW, and Chicxulub Working Group (1999) Ringed structural zones with deep roots formed by the Chicxulub impact. *Journal of Geophysical Research* 104: 10743–10755. b1600
Spector A (1968) *Spectral Analysis of Aeromagnetic Data*. PhD Thesis, University of Toronto. b1605
Spector A and Grant FS (1970) Statistical models for interpreting aeromagnetic data. *Geophysics* 35: 293–302. b1610
Shuey RT and Pasquale AS (1973) End corrections in magnetic profile interpretation. *Geophysics* 38: 507–512. b1615
Shure L, Parker RL, and Backus GE (1982) Harmonic splines for geomagnetic modelling. *Physics of the Earth and Planetary Interiors* 28: 215–229. b1620
Stone VCA, Fairhead JD, and Oterdoom WH (2004) Micromagnetic seep detection in the Sudan. *The Leading Edge* 23: 734–737. b1625
Syberg FGR (1972) A Fourier method for the regional-residual problem of potential fields. *Geophysical Prospecting* 20: 47–75. b1630
Talwani M (1965) Computation with the aid of a digital computer of magnetic anomalies caused by bodies of arbitrary shape. *Geophysics* 30: 797–817. b1635
Tanaka A, Okubo Y, and Matsubayashi O (1999) Curie point depth based on spectrum analysis of the magnetic anomaly data in East and Southeast Asia. *Tectonophysics* 306: 461–470. b1640
Tarlowski C, *et al.* (1996) Dewarping the composite aeromagnetic anomaly map of Australia using control traverses and base stations. *Geophysics* 61: 696–705. b1645
Taylor PT and Frawley JJ (1986) Magsat anomaly data over the Kursk region, USSR. *Physics of the Earth and Planetary Interiors* 45: 5–15. b1650
Taylor PT and Ravat D (1995) An interpretation of the Magsat anomalies of central Europe. *Applied Geophysics* 34: 83–91. b1655
Teskey DJ, Hood PJ, Morley LW, *et al.* (1993) The aeromagnetic survey program of the Geological Survey of Canada; contribution to regional geological mapping and mineral exploration. *Canadian Journal of Earth Sciences* 30: 243–260. b1660
Thebault E, *et al.* (2006) Revised spherical cap harmonic analysis (R-SCHA): Validation and properties. *Journal of Geophysical Research* 111: doi:10.1029/2005JB003836. b1665
Thompson DT (1982) EULDPH-A technique for making computer-assisted depth estimates for magnetic data. *Geophysics* 47: 31–37. b1670
Thurston JB and Smith RS (1997) Automatic conversion of magnetic data to depth, dip, and susceptibility contrast using the SPI™ method. *Geophysics* 62: 807–813. b1675
Thurston JB, Smith RS, and Guillon J-C (2002) A multimodel method for depth estimation from magnetic data. *Geophysics* 67: 555–561. b1680

b1685 Toft PB and Haggerty SE (1988) Limiting depth of magnetization in cratonic lithosphere. *Geophysical Research Letters* 15: 530–533.

b1690 Toft PB and Haggerty SE (1989) Reply: Limiting depth of magnetization in cratonic lithosphere. *Geophysical Research Letters* 16: 480–482.

b1695 Treitel S, Clement WG, and Kaul RK (1971) The spectral determination of depths to buried magnetic basement rocks. *Geophysical Journal of the Royal Astronomical Society* 24: 415–428.

b1700 Trumbull RB, *et al.* (2004) Aeromagnetic mapping and reconnaissance geochemistry of the Earth Cretaceous Henties Bay-Outjo dike swarm, Etendeka Igneous Province. *Journal of African Earth Sciences* 40: 17–29.

AU79

b1705 Vacquier V, Steenland NC, Henderson RG, and Zieta I (1951) Interpretation of aeromagnetic maps. *Geological Society of America, Memoir* 47.

AU81

b1710 Vallée MA, Keating P, Smith RS, and St-Hilaire C (2004) Estimating depth and model type using the continuous wavelet transform of magnetic data. *Geophysics* 69: 191–199.

b1715 Vasicek JM, Frey HV, and Thomas HH (1988) Satellite magnetic anomalies and the Middle America trench. *Tectonophysics* 154: 19–24.

b1720 Verhoef J, *et al.* (1996) Magnetic anomalies of the Arctic and North Atlantic Oceans and adjacent land areas. *Geological Survey of Canada Open file Report 3125*, Dartmouth, Nova Scotia.

AU80

b1725 Verrier V and Rochette P (2002) Estimating peak currents at ground lightning impacts using remanent magnetization. *Geophysical Research Letters* 29: doi: 10.1029/2002GL015207.

b1730 Vine FJ and Matthews DH (1963) Magnetic anomalies over oceanic ridges. *Nature* 199: 947–949.

b1735 Vivier F, Maier-Reimer E, and Tyler RH (2004) Simulations of magnetic fields generated by the Antarctic circumpolar current at satellite altitude: Can geomagnetic measurements be used to monitor the flow? *Geophysical Research Letters* L10306: doi: 10.1029/2004GL019804.

b1740 Von Frese RRB, Hinze WJ, Olivier R, and Bentley CR (1986) Regional magnetic anomaly constraints on continental breakup. *Geology* 14: 68–71.

b1745 Voorhies CV, Sabaka TJ, and Purucker M (2002) On magnetic spectra of Earth and Mars, *Journal of Geophysical Research-Planets,* 107(E6): 5034 doi: 10.1029/2001JE001534.

b1750 Wang X and Hansen RO (1990) Inversion for magnetic anomalies of arbitrary three-dimensional bodies. *Geophysics* 55: 1321–1326.

Warner RD and Wasilewski PJ (1997) Magnetic petrology of arc xenoliths from Japan and Aleutian Islands. *Journal of Geophysics Research* 102: 20225–20244. b1755

Wasilewski PJ and Mayhew MA (1992) The Moho as a magnetic boundary revisited. *Journal of Geophysics Research* 19: 2259–2262. b1760

Weinberg RF, Hodkiewicz PF, and Groves DI (2004) What controls gold distribution in Archean cratons? *Geology* 32: 545–548. b1765

Wells RE, Weaver CS, and Blakely RJ (1998) Fore-arc migration in Cascadia and its neotectonic significance. *Geology* 26: 759–762. b1770

Werner S (1955) Interpretation of magnetic anomalies of sheet-like bodies. Sver. Geol. Undersok. Serv. C. Arsbok 43: No. 6. b1775 AU81a

Wessell P and Smith W (1998) New, improved version of Generic Mapping Tools released. *EOS Transactions of the American Geophysical Union* 79: 579. b1780

Whaler KA (1994) Downward continuation of Magsat lithospheric anomalies to the Earth's surface. *Geophysical Journal International* 116: 267–278. b1785

Whaler KA and Langel RA (1996) Minimal crustal magnetizations from satellite data. *Physics of the Earth and Planetary Interiors* 48: 303–319. b1790

Whaler KA, Langel RA, Jackson A, and Purucker ME (1996) Non-uniqueness in magnetization: Crustal models from satellite magnetic data. *EOS Transactions of the American Geophysical Union* 77: F172. b1795

Whaler K and Purucker M (2005) A spatially continuous magnetization model for Mars. *Journal of Geophysical Research* 110: NO. E9, E09001, http://dx.doi.org/10.1029/2004JE002393. b1800

Wonik T, *et al.* (2001) Magnetic anomaly map for northern, western, and eastern Europe. *Terra Nova* 13: 203–213. b1805 AU83

Yanovsky BM (1938) Variations in elements of terrestrial magnetism in an anomalous field. *Trans (Trudy) Main Geophysical Observatory* 17(3). b1810 AU81b

Zietz I and Andreasen GE (1967) Remanent magnetization and aeromagnetic interpretation. In: *Mining Geophysics, Society of Exploration Geophysics*, vol. 2, pp. 569–590. Tulsa, OK. b1815 AU82

Zietz I and Bhattacharyya BK (1975) Magnetic anomalies over the continents and their analyses. *Reviews of Geophysics and Space Physics* 13: 176–215. b1820

Zietz I (1982) Composite magnetic anomaly map of the United States; Part A, conterminous United States: US Geological Survey Geophysical Investigations Map GP-954-A, 59pp, 2 sheets, scale 1:2,500,000 b1825

Author's Contact Information

AU1 **M. E. Purucker**
Raytheon ITSS at Planetary Geodynamics Laboratory
Goddard Space Flight Center, NASA
Code 698
Greenbelt
MD 20771
USA

K. A. Whaler
School of Geosciences
Grant Institute
West Mains Road
Edinburgh EH9 3WJ
UK

Keywords: Crust; Lithosphere; Magnetism; Magnetic fields; Mathematical techniques

Abstract

Crustal magnetic fields were first measured systematically by airborne surveys in the 1930s. Ground-based surveying had been developed much earlier as a tool for mineral exploration. Today, crustal magnetic fields are also measured in boreholes, from ships and balloons, and from terrestrial and planetary spacecraft. Metamorphism, petrology, and redox state all have important effects on the magnetism of crustal materials. Mapping of the crustal magnetic field provides a third dimension to surface observations of the Earth's composition and geologic structure, and a suite of mathematical tools has been developed to assist with this interpretation. Studies of crustal magnetism have contributed to geodynamic models of the lithosphere, geologic mapping, and petroleum and mineral exploration. Inferences from crustal magnetic fields, interpreted in conjunction with other information, can locate kimberlite pipes, impact structures, and other geologic entities which have a magnetic contrast with their surroundings. Present-day efforts are focused on (1) the development of a global, near-surface map of the crustal magnetic field that integrates airborne and satellite coverage, (2) extending the techniques to the other planets and moons of our solar system, and (3) extending regional and detailed mapping of the crustal magnetic field as an exploration and reconnaissance tool.